THESIS

DEVELOPMENT AND VALIDATION OF AN OUTDOOR LOW-COST SMOKE MONITOR

Submitted by

Scott Kelleher

Department of Mechanical Engineering

In partial fulfillment of the requirements

For the Degree of Master of Science

Colorado State University

Fort Collins, Colorado

Summer 2017

Master's Committee:

Advisor: John Volckens

Shantanu Jathar
Georgiana Brooke Anderson
Jeffrey Pierce

ABSTRACT

DEVELOPMENT AND VALIDATION OF AN OUTDOOR LOW-COST SMOKE MONITOR

Wildfires and prescribed fires produce emissions that are harmful to human health. These health effects, however, are difficult to quantify, likely in part due to sparse data on exposure. The ability to measure fire emissions as they reach sensitive areas is critical to ensuring the protection of public health. Ground level quantification of smoke from wildfires and prescribed fires has proven to be a difficult task. The state of the art for monitoring outdoor air quality has long relied upon expensive, cumbersome equipment that generally requires line power. Few ground-based measurements are typically made during fire events, which limits our ability to quantify and assess the impact of smoke from fire events.

The objective of this work was to develop and validate a new type of outdoor air quality monitor, the Outdoor Aerosol Sampler (OAS). The OAS is an active, filter-based air sampler that has been miniaturized and weatherproofed. The OAS represents and attempt to address the technical limitations of field sampling with a device that is relatively inexpensive and independently powered. Prototype development of the OAS was made possible through low-cost electronics, open-source programming platforms, and in house fabrication methods. An online $PM_{2.5}$ sensor was selected and integrated with the OAS. A Monte Carlo simulation aided in the selection of battery and solar power necessary to independently power the OAS, while keeping cost and size to a minimum. Cellular communications established via Short Message Service (SMS) technology were utilized in transmitting online sensor readings and controlling the OAS remotely.

Numerous OAS were deployed to monitor smoke concentrations downwind from a large prescribed fire. Mass concentrations sampled from the burn were interpolated to depict smoke concentration gradients downwind of the fire. Field tests found OAS solar charging efficiency (6.7%) to be slightly less than model input efficiency (7.5%). Outdoor urban testing of the OAS demonstrates moderate agreement with equivalent federal reference method samplers for gravimetric analysis of $PM_{2.5}$.

ACKNOWLEDGEMENTS

I would like to thank my advisor John Volckens for giving me the opportunity to work on this project and his mentoring during my time as a graduate student. I also want to thank Casey Quinn, and Dan Miller-Lionberg for their guidance and help. I'd like to thank the following Volckens group members for their assistance with this project; Josh Smith, John Mehaffy, Nick Good and Christian L'Orange. Special thanks to our partners with CDPHE, Sarah Gallup, Pat Mcgraw, and Ken Helkoski and also USFS partner John Godson.

Additional thanks are necessary towards John Volckens, Georgiana Brooke Anderson, Shantanu Jathar, and Jeffrey Pierce for being on my research committee and taking the time to help in reviewing this document.

Funding for this research was provided by the Joint Fire Science program award number 16-2-01-3

TABLE OF CONTENTS

LIST OF TABLES

LIST OF FIGURES

CHAPTER 1. INTRODUCTION

1.1 Fire Smoke Emissions

The quality of the air we breathe has an enormous impact on our health and wellbeing. Air quality is often degraded due to the presence of airborne particulate matter (PM). These fine particles can range in size from 100μm to 1nm [1] and can be anything from dust to combustion emissions with complex chemistry [2]. Fine particles measuring 2.5 micrometers and smaller in aerodynamic diameter are referred to as $PM_{2.5}$.

Exposure to $PM_{2.5}$ is harmful to human health and a major risk factor for premature mortality from cardiopulmonary diseases and lung cancer [3]. The 2015 Global Burden of Disease study estimated that $PM_{2.5}$ is responsible for 3.3 million premature deaths worldwide annually [4]. Epidemiologic studies have demonstrated that the incidence of respiratory diseases increases by 2.07% [5], hospitalization rates increase by 8% [6], and mortality increase by 4% [7] in regions where daily $PM_{2.5}$ concentrations are elevated by $10\mu g/m^3$.

The Air Pollution Control Act passed in 1955 was the first federal legislation involving air pollution in the United States [8]. The Clean Air Act of 1963 was enacted to address air pollution related to environmental problems. Major amendments to the Clean Air Act were made in 1970, 1977 and 1990. The amendment in 1990 required the Environmental Protection Agency (EPA) to set National Ambient Air Quality Standards (NAAQS). In 1997, the EPA specified that $PM_{2.5}$ mass concentrations averaged over a 24-hour period were not to exceed $65\mu g/m^3$. The acceptable daily limit was then lowered to 35 $\mu g/m^3$ in 2006 where it remains today. As a result of these legislative actions, the national average of $PM_{2.5}$ concentrations in the U.S. decreased by 37% between 2000 and 2015 [9]. Despite these regulatory efforts, PM-generating sources such as wildfires and prescribed burns still significantly contribute to the degradation of air quality. Wildfires do not fall under regulatory statutes; they are also extremely difficult to control. Wildfires and prescribed fires account for 27% of all $PM_{2.5}$ primary emissions in the United

States, making biomass burning from wildfires and prescribed fires the largest primary emission contributor [10] (Figure 1-1).

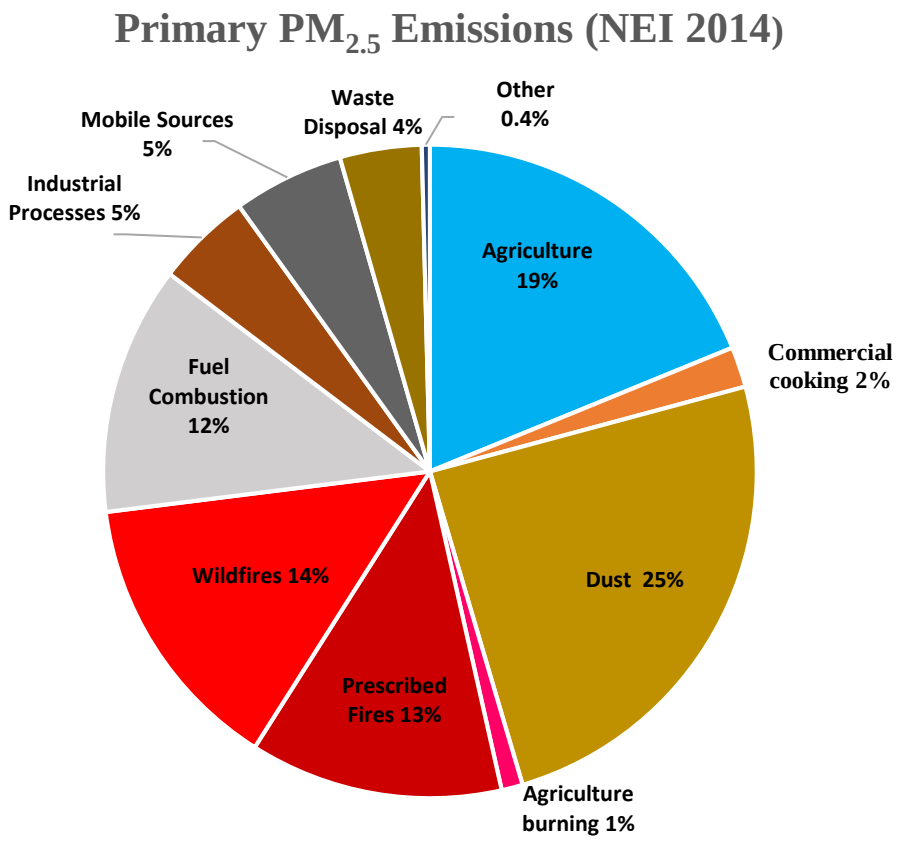

Figure 1-1. National Emissions Inventory (NEI) of Primary $PM_{2.5}$ emissions broken down by source for 2014 [10].

Particles generated from the burning of biomass are estimated to be responsible for 5% of premature deaths worldwide [4]. In addition to mortality, symptoms associated with exposure to biomass burning emissions include numerous pulmonary (asthma, bronchitis, COPD) [11-13] and cardiovascular (high blood pressure, stroke, arrhythmia) diseases [14-16].

The magnitude and chemical composition of fire emissions depend on fire behavior and a wide range of fuel characteristics like fuel type, structure, loading, composition, and moisture content. These fuel

variables are seasonal and specific to a given eco-system [17]. Given the high number of variables involved, predicting the composition and amount of pollution a fire will generate is difficult. Accurate prediction of an emission dispersion path is also complicated by dynamic meteorological variables like wind and atmospheric stability.

1.2 Fire Regime

The fire regime in the western United States has been transformed during the last century due to climate change, land-management techniques, agriculture, and the development of industry [18]. Fire has an important role in maintaining the health and long term stability of an ecosystem [19]. Climate change and aggressive fire suppression efforts to preserve structures and property have disrupted the natural effects of fire on the environment [18]. Over the past three decades, wildfires have increased in number, size and severity. This upward trend of wildfire activity is predicted to persist in coming years [20], meaning biomass burning in the United States will have an even greater impact on public health and ecosystems in the future. Not including the emissions generated from prescribed burns, wildfires themselves are estimated to become the largest contributing source of $PM_{2.5}$ in the United States by 2050. Yearly average of area burned is predicted to increase by 54% and carbonaceous aerosol emissions are expected to double from 2000 to 2050 [21, 22]. A trend of increased wildfire activity (acres burned) in the US from 1985 to 2015 is shown in Figure 1-2A; increasing yearly quantity of acres burned by prescribed fire is shown in Figure 1-2B.

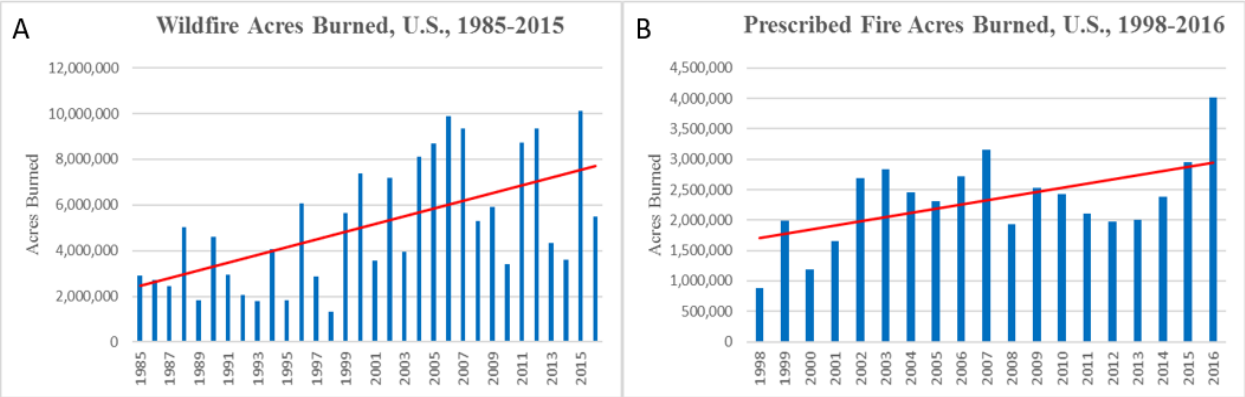

Figure 1-2. (A) Acers burned by wildfire in the United States from 1985-2015 [23], (B) Acres burned by prescribed fire in the United States from 1998-2016 [24].

One method of wildfire prevention is prescribed burning. In the late 1990's, land managers and landowners increasingly used fire as a tool in the application of prescribed burns (well above normal annual levels at the time). As a result, the Interim Air Quality Policy on Wildland and Prescribed Fires was written by the EPA in 1998 to preserve public health and wellbeing by mitigating the air quality impacts from these emissions. The majority of PM produced by prescribed fires is $PM_{2.5}$ [25]. Particulate size distributions largely depend on fuel characteristics, meteorological conditions, fire intensity and mass flux of emissions. Combustion of wildland fuels produces particles that typically follow a lognormal size distribution (sometimes bimodal) with an unaged submicron count median diameter of (35-120 nm) and geometric standard deviation of around 1.6 [26, 27]. Prescribed burning is a powerful tool, however very little is known about air pollution impacts that follow these events.

Wildfires are exceptional events that are difficult to control. Both wildfires and prescribed burns generate $PM_{2.5}$ concentrations that can exceed the $35\mu g/m^3$ National Ambient Air Quality Standards in close proximity as well as substantial distances away from the fire [28]. Wildfire emissions that elevate particulate mass concentration enough to exceed National Ambient Air Quality Standards (NAAQS) are not considered violations of the Clean Air Act provisions. Nonetheless, these emissions pose harmful implications to human health.

Health effects from anthropogenic ambient $PM_{2.5}$ are well studied and documented, however, the health effects directly associated with pollution from fires are not as well known. Community smoke exposures from wildfires have been associated with increased hospital admissions for chronic obstructive pulmonary disease, bronchitis, asthma, and chest pain [29]. Sensitive groups such as children and the elderly may be at particularly high risk of experiencing adverse health outcomes if exposed to the high levels of air pollution associated with fire events [30]. A better understanding is needed on smoke emissions and exposures from wildfires and prescribed burning events. Prescribed burn managers utilize smoke mitigation techniques to minimize the impacts from smoke and keep emissions levels below the NAAQS threshold. Evaluating the effectiveness of smoke mitigation techniques is often difficult to assess due to spatially sparse monitoring.

1.3 Monitoring

The ability to track and quantify fire emissions as they reach sensitive areas (such as homes, schools, and hospitals) is critical to ensuring the protection of public health [25, 26]. Quantifying the timing, location, and severity of these emissions at the ground level with high spatial resolution rarely happens due to a lack of monitoring instrumentation. Conventional instruments used for wildfire $PM_{2.5}$ monitoring [31] are expensive, typically $10,000 to $30,000 per unit [32, 33]. These instruments are large and ordinarily require line power; thus, sampling sites are often confined to locations equipped with utility service and accessible by motor vehicle. Only a small number of measurements are made during most fire events, which often results in an incomplete representation of the fire's impact on air quality [34].

Ground-based measurements of $PM_{2.5}$ are routinely made throughout the United States using federal reference method (FRM) or federal reference method equivalent (FEM) monitors. A list of federal reference method monitors is available from the EPA [35]. The EPA consolidates measurements taken from local, state, and federal monitors into the EPA Air Quality System [36]. FRM and FEM monitors typically utilize one of three approved techniques for PM measurement: optical, gravimetric, or beta attenuation. Optical measuring devices (nephelometers, photometers, and optical particle counters) use light scattering based principles (Mie scattering) to quantify aerosol mass concentration and typically report hourly data with

immediate availability. State-of-the-art light scattering devices correlate well with gravimetric reference samplers when calibrated to the specific aerosol being sampled. However, nephelometers can yield erroneous measurements if not calibrated for specific aerosol size, density, and refractive index [37]. Nephelometers are also subject to additional mass measurement bias due to the condensational growth of particles associated with water adsorption by hygroscopic PM [38].

Gravimetric samplers draw air through a filter, depositing PM onto the filter. The filter is weighed before and after sampling to estimate accumulated mass. The mass gained by the filter is then used with sampler flow rate and sampling duration to calculate an average mass concentration during the time of sampling. Gravimetric FRM samples are typically collected on a daily or every-third-day basis. Results from gravimetric samplers are not available until 4-6 weeks following sample collection. Gravimetric sampling is labor intensive. Filters must be conditioned, weighed prior to sampling, installed, collected, reconditioned and weighed again after sampling on a highly sensitive scale. Flow rates and sampling time need to be closely monitored to ensure accurate results.

Another FRM gravimetric-based sampler, called a Tapered Element Oscillating Microbalance (TEOM), operates by a coil driver pulsating against a tapered filter element to maintain an oscillatory motion. As air is drawn through the oscillating filter element, PM mass accumulates onto the filter and oscillation frequency decreases [39]. The change in frequency with respect to time is measured by a Hall Effect sensor and related back to PM mass concentration. This measurement method allows the TEOM to provide a direct mass measurement with excellent sensitivity for particles with varying properties (density, size, refractive index). Due to the TEOM's sensitivity to humidity and temperature, filters are maintained at 50 °C. Heating the filters to this temperature can result in the evaporation of semi-volatile species, resulting in a negative bias to measured mass [40]. Filter elements within a TEOM need to be exchanged periodically.

The Beta Attenuation Monitor (BAM) measures particulate mass by quantifying absorption of ionizing radiation by particles. BAM monitors collect PM by drawing air through a filter material. The filter material is subjected to a beta source emitter. A detector on the other side of the filter measures, by difference, the

amount of beta radiation attenuated by the particles, which is related to PM mass on the filter material according to a Beer-Lambert relationship. Given the volume or air drawn through the filter and the degree of beta attenuation, a mass concentration is calculated. This measurement is repeated every hour with immediate results. The BAM measurement is based on mass only; particle density, chemical composition, and optical properties do not influence the measurement.

Ground-based FRM monitors are sparsely located throughout the US, especially the western US, leaving large spatial gaps in air quality data. This spatial data void limits the amount with which concentration gradients of fine particulate matter at the ground level can be resolved. A map of Colorado's 20 self-reporting $PM_{2.5}$ monitors is shown below in Figure 1.3. Monitors are largely concentrated on the Front Range of Colorado with respect to the rest of the state. The monitors in densely populated areas like Denver are tens-of-kilometers apart while more rural monitors are often separated by hundreds of kilometers.

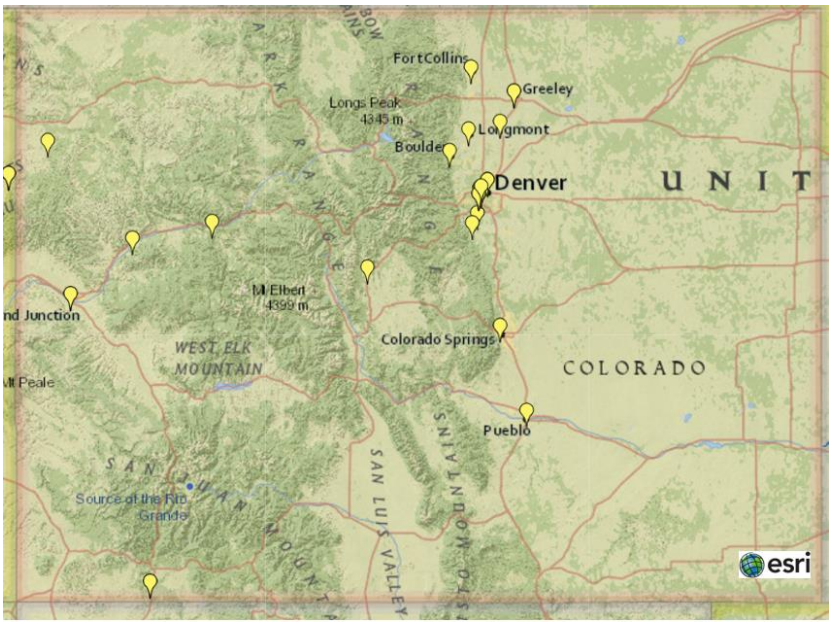

Figure 1-3 Map showing the location of each active $PM_{2.5}$ monitor in the state of Colorado. Data from [41], Sources: (Esri, DeLorme, HERE,USGS, Intermap, iPC, NRCAN, GEBO,NOAA, iPC)

Satellite observations of air quality can be utilized to provide assistance in satisfying ground based monitoring gaps. MODerate resolution imaging spectroradiometer (MODIS) instrumentation, aboard the Terra and Aqua satellites, yield daily aerosol optical depth (AOD) measurements worldwide. AOD is an integrated extinction of light from the total mass of aerosol present in a vertical column of the atmosphere; thus, AOD includes total aerosol mass at all elevations. The measurements taken by satellite are not always representative of $PM_{2.5}$ at the ground level. An in-depth evaluation and explanation of satellite aerosol monitoring technology can be found at the following sources [42,[42]. Tools like USFS BlueSky, NOAA HMS and EPA AirNow are other useful tools for evaluating air quality. However, like satellite AOD observations, these tools lack fine spatial resolution and do not quantify air quality specifically at ground level. Health and risk assessment studies rely on models that use PM surface observations in combination with other remote monitoring tools (e.g. satellite based AOD and chemical transport models) to evaluate exposure. However, these models are limited by the number of surface observations available, thus limiting the power of the assessment [43].

The U.S. EPA's Policy, taken from the Interim Air Quality Policy [25] on Wildland and Prescribed Fires, states that *"Wildland and air quality managers should work with the press to announce pre-fire health advisories, and post-fire results including such things as the management objectives met; smoke intrusions observed, and/or successful minimization of air quality impacts."* Given the current state of the art, comprehensive monitoring of fire emissions is neither affordable nor practical for burn agencies. Research and development on inexpensive air quality monitoring technology is rapidly increasing. Several recent studies investigate indoor air pollution using off-the-shelf, low-cost sensors (e.g. [44-46]). Even fewer studies have been done on outdoor air quality using low-cost sensors.

An example of a low-cost mobile air quality sensor for wildfires, currently in development and testing stages, presented at IAWF's 2nd International Smoke Symposium can be found here [47]. Most low-cost air quality sensors available for use in outdoor sampling are strongly influenced by meteorological elements. Temperature dependence and humidity bias are known to exist for most low-cost particulate matter sensors [38, 48, 49]. Signals from these sensors are generally noisy, requiring the application of averaging and

smoothing techniques. Fire emission monitoring requires sensors to be quite robust and self-governing. These factors combined make outdoor sampling with low-cost sensors challenging.

1.4 Objectives

The overall goal of this project was to develop and validate a field-deployable, low-cost (under $500) $PM_{2.5}$ sampler that can run autonomously with no external power. The sampler was intended to be remotely programmable and encapsulated in a lightweight, hardened enclosure. Specific design and performance objectives for the unit were: weigh less than 900 grams (2lbs), fit within a 3000cm^3 (183 in^3) volume, weatherproof, powered by solar and rechargeable battery, capable of providing both online (via light scattering) and time integrated (via size-selective sampling onto a filter) measurements of $PM_{2.5}$, and capable of long deployments (up to 2 weeks of continuous measurements). Following instrument development, a network of low-cost $PM_{2.5}$ monitors was deployed downwind from a prescribed fire to evaluate the performance of this monitor as a smoke-monitoring tool. Additional deployments were also conducted at FEM monitoring sites along the Northern Front Range of Colorado to evaluate monitor performance at typical ambient $PM_{2.5}$ concentrations.

CHAPTER 2. METHODS

2.1 UPAS Technology

The Volckens research group at Colorado State University recently developed an Ultrasonic Personal Aerosol Sampler (UPAS) [50]. The Outdoor Aerosol Sampler (OAS), the focus of this thesis, was based upon the UPAS technology. The UPAS is a wearable device designed to estimate personal exposure to $PM_{2.5}$ across a 24-hour period. A key feature of this sampler is an ultrasonic pump that provides reductions in size, cost, and power relative to existing diaphragm or rotary-vane air sampling pumps. The UPAS, shown in Figure 2-1a, weighs 190 grams and has a bill-of-materials of approximately $300. The sampler contains a size-selective cyclone inlet for $PM_{2.5}$, a 37-mm air sampling filter, rechargeable batteries, a suite of environmental sensors (location by GPS, temperature, pressure, relative humidity, acceleration, light, and a real-time clock), and a miniature mass-flow sensor. Flow-rate through the instrument can be programmed between one and two liters per minute.

In prior laboratory tests, the UPAS performed well compared to both an EPA $PM_{2.5}$ federal reference method (URG cyclone model URG-2000-30EGN-A; URG Corp., Chapel Hill, NC, USA) and a personal $PM_{2.5}$ sampler (PEM 761-203; SKC, Inc., Eighty Four, PA, USA). The UPAS cyclone has a collection efficiency that complies with the EPA $PM_{2.5}$ criterion standard. Shown in Figure 2-1a is an image of the original UPAS design; the performance of the UPAS pump at three different (arbitrary) power levels is shown in Figure 2-1b. These pump performance data allow UPAS power consumption to be estimated as a function of flow and filter type.

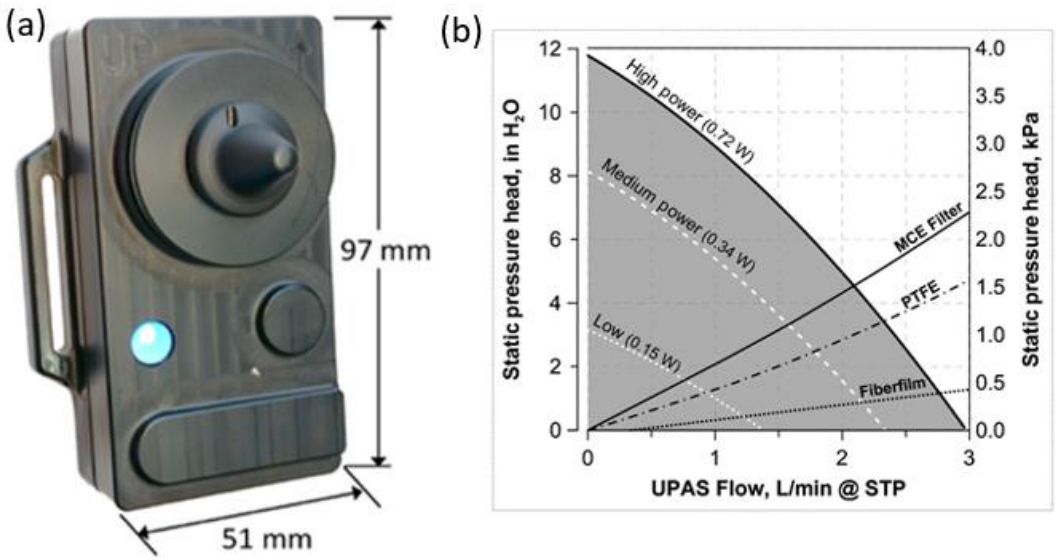

Figure 2-1. (a) The original UPAS device; (b) UPAS pump performance curve and filter pressure drop vs flow rate. Three UPAS power levels and three different 37- mm filters types are shown: mixed cellulose ester (MCE; 0.8 µm SKC, Inc.), polytetrafluoroethylene (PTFE; PT37P, MTL Inc.), and PTFE-coated glass fiber (Pallflex Fiberfilm; Pall Inc.) [38]

With the exception of the cyclone inlet, housing, and circuit board, the internal components of the UPAS are all 'other equipment manufacturer' (OEM) components available on the commercial electronics market. The battery life for this device is approximately 20 hours at a flow rate of two liters per minute. A published manuscript on the development and evaluation of the UPAS can be found at [50].

2.2 Development

The following additions and modifications were made to convert the UPAS from an indoor personal exposure sampler to an outdoor air sampler: a) Add an online $PM_{2.5}$ sensor; b) Add cellular communication (Short Message Service, SMS); c) Extend battery life through additional battery and solar power and; d) Harden the enclosure for all-weather operation.

In addition to the modifications listed above, a few minor alterations to the UPAS sampler itself were made. A modified size selective inlet combined with a filter cartridge and threaded aluminum cap made

the UPAS more user friendly and robust. A machined plastic housing was also designed to allow the UPAS to be mounted directly into a weatherproof case.

A literature review was conducted to identify a low-cost light-scattering device to serve as an online $PM_{2.5}$ sensor for the OAS. The selection was based on performance criteria with respect to other low-cost air quality sensors outlined in [49]. Candidate sensors were evaluated according to the following figures of merit: linearity of response, precision of measurement, accuracy, repeatability, limit of detection, dependence on compositions, sensitivity to particle size, relative humidity influence, and temperature influence. The $PM_{2.5}$ sensor selected for this work was the Sharp GP2Y1023AU0F. The Sharp is primarily comprised of a light emitting diode (LED), two lenses, and a photodiode. The LED produces light which is focused through a lens and directed through a sample of air. The amount of light scattered, via Mie scattering, is detected by a photodiode positioned behind a lens, approximately 60 degrees offset from the LED. The Sharp is a passive sensor (it does not use a fan or pump to draw air for sampling), which allows for less power consumption. For this application, outdoor air convection (i.e., wind) was expected to provide sufficient air exchange for the sensor. Thus, the Sharp was mounted on the underside of the solar array to provide shielding from rain while also providing unrestricted access to open air. According to the manufacturer's specification sheet, the Sharp outputs a voltage linearly related to PM mass concentration.

The OAS is a mass-based, time-integrated monitor geared primarily toward assessing population's cumulative risk of PM exposure. When originally conceived, the real-time light scattering PM sensor (Sharp) integrated into the OAS was envisioned to serve as a trigger mechanism as well as a real-time sensor. The measurement from the real-time sensor would prompt the OAS to begin sampling gravimetrically once a threshold of aerosol concentration was exceeded. The prompt from the real-time sensor would serve as an early warning alarm (transmitted via onboard SMS technology) for an approaching smoke plume. Using the real-time sensor as a trigger allows the OAS to remain idle until a smoke plume is present, thus conserving battery life of the instrument. Thus, the OAS was designed to capture both spatial and temporal impacts of wildfire smoke emissions.

Preliminary outdoor testing of the Sharp revealed the sensor's sensitivity to meteorological conditions. To dampen the impact of meteorological variables on the Sharp's measurements, several Sharp sensors were co-located with a DustTrak DRX (TSI Inc., Shoreview, MN, USA) for a week in an outdoor setting. During this time, temperature, atmospheric pressure, relative humidity, Sharp output signal, and DustTrak measurements were recorded. A multivariate polynomial regression (MFP package in R) was used to produce an equation describing the relationship between meteorological variables and the ratio of Sharp output to DustTrak measurements.

The addition of remote communications with autonomous operation was accomplished by adding Short Message Service (SMS) technology. This cellular technology allowed the OAS to be controlled via cell phone (or any device with internet access) and report real-time measurements to the user. The built-in SMS technology and predesignated communication protocol of a Particle Electron (Particle Industries Inc., San Francisco, CA) was utilized for remote communications. The Electron also features a microcontroller that was integrated into the UPAS circuitry.

The Electron connects to Particle's web application program interface (API) using the Global System for Mobile Communications (GSM). The Electron can then send information to the Particle server, where it is hosted on a web page specific to each device. The URL of this web page is determined by the active particle account, board ID number and function type. The Electron maintains communication with the Particle server, allowing any internet connected device to access the web page URL. An access token was in place for security purposes, preventing any unauthorized access.

An HTML file (ran as a webpage) was used to display incoming OAS network information as well as to send remote commands to the OAS. The HTML featured a set of user friendly controls, that when activated, would post to the Particle API. The Electron would then receive the command by communicating with the Particle server over GSM. A Google Script was utilized for harvesting the information cached on the Particle server every hour, where it was then logged to a Google Sheet and displayed on the HTML page.

Three, 12-volt, solar cells mounted on a weatherproof housing (described below) were leveraged to make the OAS independently powered. The solar cell arrangement was designed to be collapsible to maintain a slender profile for easy transportation and shipping. A magnetically coupled bracket that is adjustable for optimum zenith-angle, holds the solar cells rigidly in place while in deployment and transportation configuration. The OAS's various configurations are represented in Figure 2-2. The OAS battery charge controller required a voltage regulator to condition electricity from the solar cells to 5 volts DC. The battery capacity was increased to 54 watt-hours through the use of 5 (10.78 watt-hour) lithium-ion batteries in parallel.

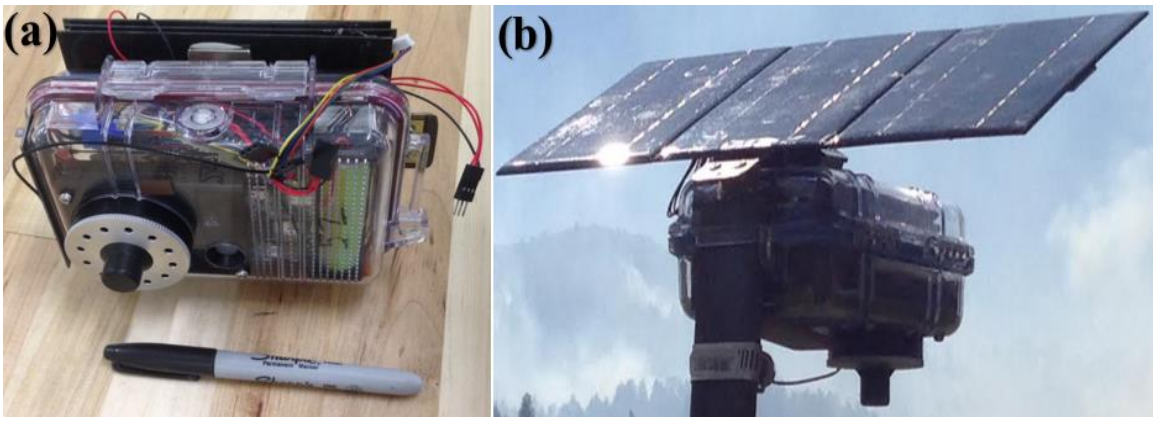

Figure 2-2. OAS sampler in (a) transportation configuration and (b) deployment configuration.

A Pelican 1020 Micro Case was modified to facilitate the UPAS and additional components. A series of small holes were bored on the underside of the case to allow the air being pumped by the UPAS to be expelled from the case. The mass-flow sensor onboard the UPAS is highly dependent on air density, which fluctuates significantly as a function of temperature. The UPAS creates a small amount of heat during operation as a byproduct of pump work. Air downstream of the pumps is routed through the Pelican case to help maintain a temperature inside the case near ambient. A complete air exchange within the case takes place on a 15 second time interval when the OAS actively pumping. Shielding provided by the solar cells reduces OAS internal heating due to the absorption of solar radiation.

Table 1 lists the various components added to the UPAS in the development of the OAS. The retail cost of these components, when purchased in single quantity, totals approximately $183. The block diagram in Figure 2-3 depicts a simplified version of the UPAS and its respective components, the components added to the UPAS for OAS development, and the interaction among components.

Table 1. Components added to UPAS to form the OAS

Component	Manufacturer	Part number	Cost
Polycrystalline Solar Cell	Banggood	991137	3@$5
Voltage Regulator	ProDCtoDC	90462	$5
Microcontroller/SMS Module	Particle	Electron 3G	$59
MicroSD card logger	Molex	5031821852	$7
Battery (2800 mAh)	Anker	7OSMS5-28N	3@$14
Temp, Pressure, RH sensor	Bosch Sensortec	BME280	$10
Current/Voltage Sensor	Texas Instruments	INA219	$10
Low-cost PM Sensor	Sharp	GP2Y1010AU0F	$8
Sharp Sensor adapter	DFRobot	DFR0280	$4
Weatherproof enclosure	Pelican	1020 micro	$14
Magnets	KJ Magnetics	BX08H1	7@1.3

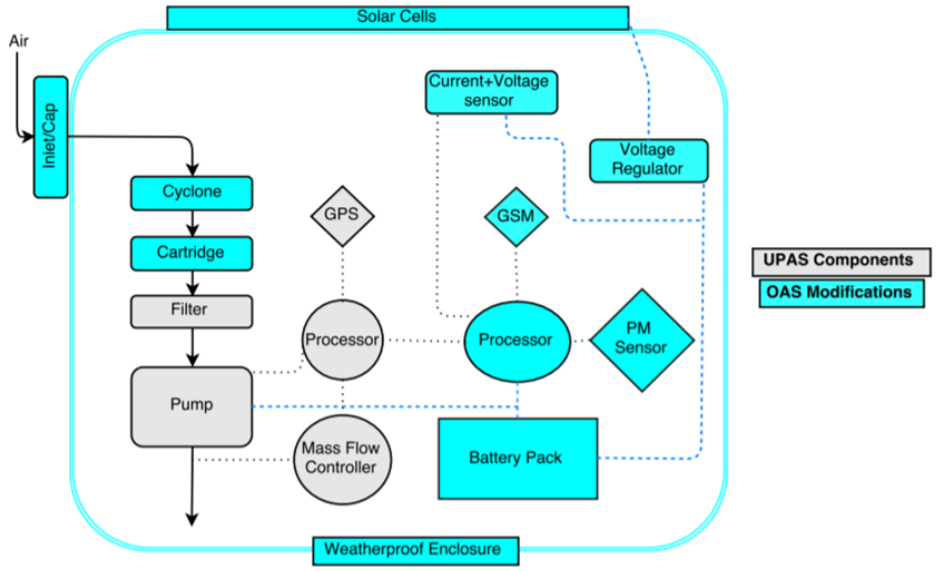

Figure 2-3. Block diagram of UPAS technology with component integration to form the OAS.

A small, steel adapter was fabricated to mount the pelican case to a standard metal T-post (Figure 2-2b). The T-post served as a study stand, elevating the OAS to a height of 1.2 m above ground level. The use of the T-post allowed for easy setup at any remote location because it is simply driven into the ground for support. An adjustable folding tripod was used for urban areas where use of a single steel post was not appropriate (e.g., on rooftops).

2.3 Power System Design

Monte Carlo simulations were used to inform the selection of OAS solar and battery power. These simulations were conducted with the following design constraints, which were based on practicality and desired functionality: (1) the OAS must weigh < 900 grams, (2) must fit in a 3000cm^3 volume (for easy shipping), and (3) the additional costs of all OAS components must be less than $150 (on top of existing UPAS costs). The simulations used solar irradiance data for Fort Collins, Colorado from 2011-2015 [51]. These data follow a mesokurtic (normal) distribution with more variability during summer months. The solar irradiance value input to the model is defined as the daily average of observed solar irradiance attuned for solar cell size (0.014m^2 each). Daily, ground-level solar irradiance is largely driven by cloud cover, time of year and weather. The model determines the probability of power failure for the OAS on a given day during each month of the year.

The model accounts for the following parameters: useable battery capacity, stationary solar conversion efficiency, temperature effects on battery capacity, charge circuit efficiency and average OAS power consumption at 2 L/min of sample flow. Power consumption will vary depending on filter loading and filter type. An OAS power consumption rate of 0.7 Watts was held constant throughout the simulations. One thousand iterations of 14-day sampling periods, for each month of the year, were simulated to calculate runtime (in days) for each iteration. The probability of power failure (for a series of consecutive sampling days across a particular month) is equal to the total number of failures specific to that day divided by the number of iterations simulated. Table 2 lists all input variables used in the simulation design. The amount of daily solar irradiance available (S), is the simulation's only Monte Carlo sampled input.

Table 2. Power design model variables

Variable	Term	Input (units)	Data Source
R	Rated Battery Capacity	10.78 (Watt-hours)	Determined
E	Solar Circuit Efficiency	7.50%	Determined
N	Battery Quantity	5 (unit less)	Determined
T	Temperature	Monthly mean of daily low	[52]
P	OAS Daily Power Consumption	16.8 (Watt-hours)	Determined
S	Solar Irradiance Available	Monte Carlo sampled daily value (watt-	[53]
V	Useable Battery Capacity Percentage	85%	Determined
C	Battery Capacity Temperature	Equation 2 (unit less)	[54]

Useable battery capacity percentage (V) was determined to be 85% based on OAS circuit cutoff voltages. Fully charged battery capacity B_0, where the subscript refers to day '0', can be expressed using Equation 1;

$$B_0 = R * N * C_i * \mathrm{V}(1),$$

where R is rated battery capacity, N is battery quantity, C_i is the capacity correction from temperature (for month i), and V is useable battery capacity percentage. The Li-ion battery capacity correction factor, C, as a function of month, i, for an 18650b battery type, is described in Equation 2;

$$C_i = (-0.0097T_i^2 + 0.8061T_i + 90)/100 \qquad (2),$$

where T(ºC) is the mean low temperature across a given month, i [54]. Equation 3 is used to calculate the runtime (in days) for each of the 1000 sampling missions each month;

$$Runtime\ (days) = \sum_{d=1}^{14} \begin{Bmatrix} 0\ if\ (B_{d-1} - P + S * E) > 0 \\ 1\ if\ (B_{d-1} - P + S * E) < 0 \end{Bmatrix} \quad (3),$$

where B is battery capacity at the conclusion of day d, P is daily OAS power consumption, S is available solar irradiance and E is solar energy conversion efficiency.

The sum of iteratively accumulated failures unique to a specific runtime (days) across all 1000 sampling missions simulated, divided by the number of iterations (1000), yields power failure probability for a given runtime that month. This calculation is repeated to calculate a failure probability for each of the 14 consecutive days that were simulated across each month of the year. Simulations were conducted

using Matlab R2015a (The MathWorks Inc., Natick, MA). The sensitivity of the Monte Carlo simulation to varying solar cell and battery quantity was evaluated by simulating battery quantity ranging from 2-5 batteries and solar cell quantity ranging from 1-3 cells. All other simulation parameters were unchanged for this sensitivity analysis.

2.4 Prescribed Fire Sampling

Partnering closely with Colorado Department of Public Health and Environment (CDPHE) and the US Forest Service (USFS), thirteen OAS were arrayed in southern Colorado during one of the largest prescribed fires in state history. The 6000-acre fire took place in Archuleta and La Plata Counties, approximately 14.5 km east of Bayfield Colorado from September 8th through September 17th 2016. Multiple days of post-burn holding operations also occurred. The primary objective of the fire was to reduce the existing wildland fire hazard by reinstating fire, increasing resistance and resiliency of the warm-dry mixed conifer and ponderosa pine forest types in this region. This burn was intended to reduce potential negative effects from future wildland fires to public and adjacent private lands while promoting a fire-adapted ecosystem [55].

The OAS network was deployed prior to fire ignition. The sampling location of each OAS was selected with guidance from on-site, USFS overseers. Leveraging the prescribed fire experience and local terrain familiarity of the USFS, each OAS was positioned in areas expected to be most impacted by smoke downwind and downslope from the fire. Other considerations and factors for sampler placement included: cooperation and permission from land owners, obstruction to fire operations, potential for livestock interference, and ease of access. To ensure measurement of emissions from burn operations only, OAS were placed a minimum of 60 m from other potential PM sources (e.g., gravel roads). The samplers were situated away from surrounding obstacles of significant height, to prevent solar interference.

The locations of thirteen OAS and two USFS monitors are shown in Figure 2-4. The USFS monitored air quality during the prescribed burn by placing instruments at Vance Ranch (E-SAMPLER, Met One Instruments) and the fire station in Arboles, Colorado (E-BAM, Met One Instruments). Two OAS were co-located with the US Forest service monitors at both Vance Ranch and Arboles Fire Station. For the duration of the fire, the OAS sampled $PM_{2.5}$ for 24 hours onto 37mm Tisch PTFE filters (model SF17382). The well

characterized Pallflex line of filters previously used with UPAS samplers was discontinued; Tisch PTFE filters were selected as an alternate. Flowrate through the OAS was set to 2 L/min. Hourly $PM_{2.5}$ and meteorological data from the E-BAM and E-SAMPLER were made publically available on Western Regional Climate Center's website (E-BAM 925, R-2 922). Twenty-four hour averages of the E-BAM and E-SAMPLER data were used for comparison with co-located OAS.

Solar energy conversion efficiency was evaluated for each OAS and across all sampling periods. Data from the voltage/current sensor (INA219) were used to determine the ratio of solar energy delivered to OAS batteries relative to available solar irradiance. Hourly irradiance measurements were provided by a weather station (PRAWS 5) located on Pargin Mountain during the month of September, 2016. Pargin Mountain weather station data is available on MOSWest's website [56]. The daily amount of runtime added to each OAS via solar is expressed in Equation 4;

$$Runtime\ added = H/F \qquad (4),$$

where H is the daily amount of solar energy harvested by the OAS (watt-hrs.) and F is average rate of OAS power consumption (0.7 watts).

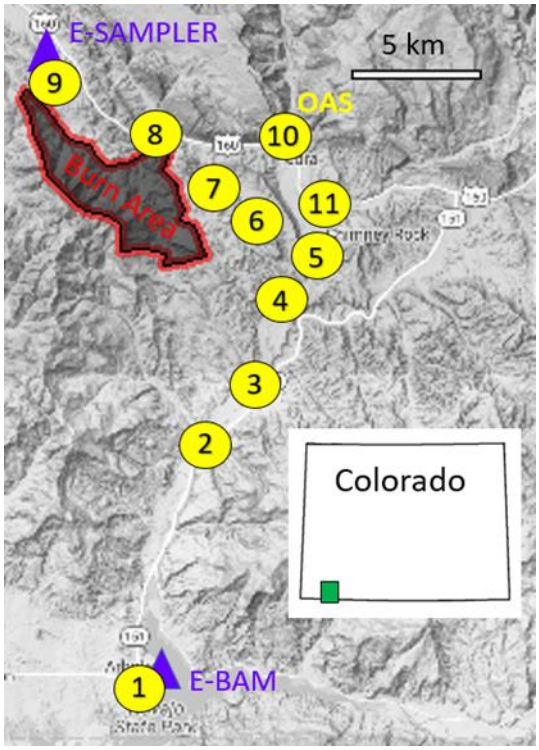

Figure 2-4. Location of monitoring equipment with respect to prescribed fire. OAS (yellow circles), US Forest Service equipment (blue triangles), prescribed fire (shaded black area with red outline).

2.5 Urban Sampling

Following the controlled burn experiment, OAS performance was evaluated through a series of outdoor deployments along the northern Front Range of Colorado from January 26th – February 16, 2017. Two OAS were co-located with Colorado Department of Public Health and Environment's FEM monitors (Grimm Model 180) at five different FEM sites (ten OAS and five FEM monitors total). The Grimm FEM is an optical particle counter that assumes an aerosol density to estimate $PM_{2.5}$ mass concentration. The Grimm Model 180 uses a vacuum Nafion dryer to reduce the bias that nephelometers normally experience at high ambient humidity [38]. More information on the Grimm 180 instrument can be found in the user's manual [57]. Four Denver-area co-location sites are shown in Figure 2-5a and the Fort Collins site is shown in Figure 2-5b.

Each OAS was set to sample for 48-hours at a flow of 2 L/min. OAS battery packs were exchanged with a fully charged battery pack between each 48-hour sampling period. Given the relatively clean air of Colorado, 48-hour sampling periods were chosen over 24-hour sampling periods to increase the mass of PM sampled. More particulate mass on the filters allows the gravimetric measurement to be made with a higher degree of certainty. Pall Teflo 37mm filters with Polytetrafluoroethylene (PTFE) membrane, polymethylpentene support ring, and 2.0 µm pore size were used in the Denver/Fort Collins FRM co-location sampling.

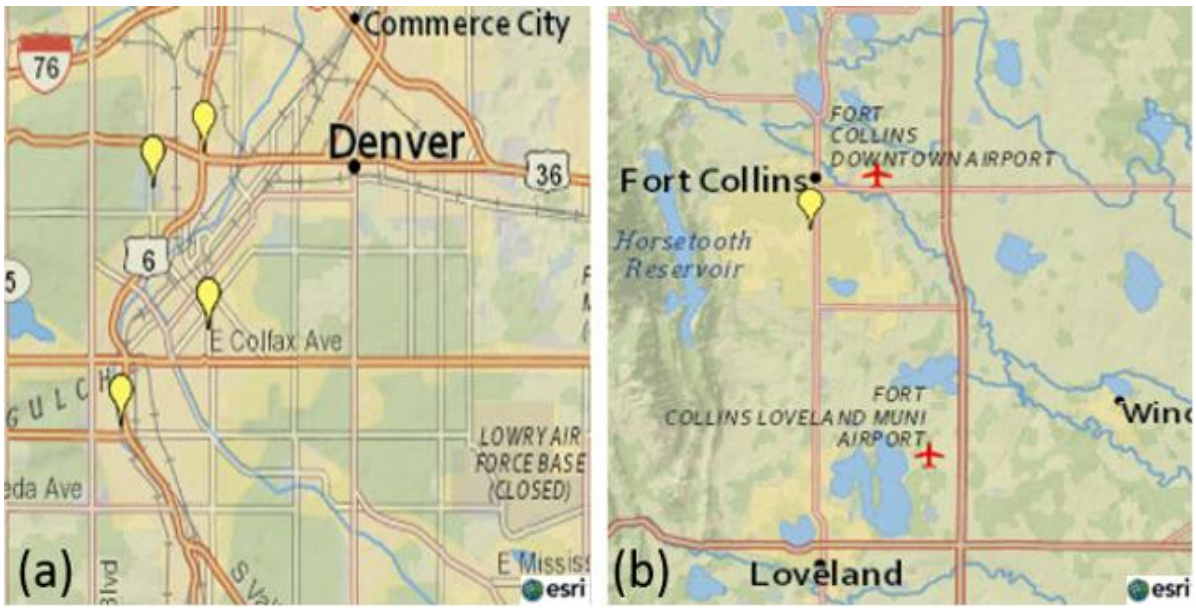

Figure 2-5. Sites of OAS and Grimm Co-location sampling. (a) Denver, Colorado (b) Fort Collins, Colorado. Data from [41], Sources: (Esri, DeLorme, HERE,USGS, Intermap, iPC, NRCAN, GEBO, NOAA, and iPC)

2.6 Analysis Methods

The following procedure was used for the prescribed fire sampling as well as the co-location evaluation tests. Flow through the OAS was checked pre and post sampling using a Mini-Buck Calibrator (A.P. Buck, Inc. Orlando, FL, USA) in conjunction with custom-made inlet adapters. A Mettler Toledo XS3DU microbalance, accurate to ± 1 µg, was used to weigh the filters. Filters were placed in an equilibrium chamber for at least 12 hours before pre- and post-weighing and discharged on a polonium-210 strip for a

minimum of 15 seconds prior to each weighing. The polonium strip brings the filters to a neutral potential so any charge that has accumulated on the filter during sampling and handling does not bias the mass measurement. Three readings were averaged together to determine each filter weight and field blanks were carried for all deployments. Following post-weigh analysis, the filters were sealed in air tight bags and stored at -20 °C.

Descriptive statistics were calculated for all mass concentration data, including identification of outliers. For the prescribed fire and FEM co-locations, outliers were defined as cases where the OAS knowingly malfunctioned. Limit of detection for gravimetric measurements was defined as three times the standard deviation of the change in mass detected on the blanks. Limit of quantification was defined as five times the standard deviation.

Data analyses were conducted using Excel 2016 (Microsoft Corp., Redmond, WA, USA), Matlab 2015 (The MathWorks Inc., Natick, MA) and R 3.3.2 (R Core Team, Vienna, Austria). Spatial interpolation and plotting of prescribed fire sampling results was performed using R packages gstat, raster, and sp. Using the fortify function (ggplot2 package), raster objects were projected onto a map layer. Spatial interpolation and plotting of prescribed fire sampling results was based on ordinary kriging methods. Model interpolations were constrained to an area (search radius) no more than 3km from a given sampler location. If not constrained, interpolated values would be calculated through vast distances with respect to OAS measurements. Incorrect assumptions would be made across large topographic barriers (like mountain ridges) that often play a large role in forming air quality concentration gradients.

Particle collection efficiency of the Tisch PTFE filters was evaluated in a 0.76 m^3 aerosol chamber; wood smoke was used to simulate prescribed fire aerosol. Chamber concentration was raised to 200 $\mu g/m^3$ initially as measured by a DustTrak DRX (TSI Inc., Shoreview, MN, USA) and then left undisturbed for the remainder of the test. A scanning mobility particle sizer (SMPS, model 3082, TSI Inc., Shoreview, MN) was used to count particles in 110 discrete size ranges from 19 to 1000 nm. A set of repeated measures was made with a filter inline and then removed (alternating the order between sets) for four test filters, three sets per filter. Additional chamber air (1.4 L/min) was metered through the filter to

make up the difference between the intended OAS flowrate (2 L/min) and the flow into the SMPS, which was nominally 0.6 L/min. Filter collection efficiency is specific to a given flow rate.

Filter collection efficiency for each particle size range was determined using equation 6;

$$filter\ collection\ efficiency_i = \eta_i = 1 - \frac{N_{i,on}}{N_{i,off}} \qquad (6),$$

where $N_{i,on}$ is the particle count measured by the SMPS with filter on, $N_{i,off}$ is the particle count measured by the SMPS with filter off and i represents the midpoint of each particle size range. Mass collection efficiency of the Tisch filter was estimated for prescribed fire aerosol using an aerosol size distribution specific to wildland fire. This distribution was modeled from a lognormal distribution having a count median diameter (CMD) of 70 nm and geometric standard deviation (σ_g) of 1.7 [27]. The mass of a single particle in each particle size range ($m_{p,i}$) was calculated using equation 7,

$$m_{p,i} = \frac{\pi}{6} d_i^3\ \rho \qquad (7),$$

where d_i is the median particle diameter for each size range, i, and ρ is particle density. The mass in each particle size range (M_i) can be calculated using equation 8,

$$M_i = N_i\ m_{p,i} \qquad (8),$$

where N_i is the number of particles present in size range i. The mass collection efficiency of the filter is determined by the ratio of particulate mass collected by the filter to total particulate mass. Percent mass collection efficiency is calculated using equation 9:

$$mass\ collection\ efficiency = \frac{\sum_{i=1}^{n} \eta_i\ M_i}{\sum_{i=1}^{n} M_i} * 100 \qquad (9),$$

where the numerator on the right hand side represents the particulate mass collected by the Tisch filter (determined experimentally) summed up over n size ranges and the denominator is the summation of particulate mass across equivalent size ranges for a hypothetical biomass burning aerosol [27].

Performance of the OAS relative to the E-BAM for prescribed-fire sampling was evaluated using a simple linear regression. Performance evaluation of the OAS relative to the Grimm samplers utilized an errors-in-variables model (Deming regression) to estimate a linear fit between methods. Deming regression

accounts for errors in both the x and y variables by minimizing the perpendicular distance between the best fit line and data points. The errors of the Grimm and OAS were assumed to be independent and normally distributed.

CHAPTER 3. RESULTS AND DISCUSSION

3.1 UPAS Modifications

Several UPAS modifications aided in streamlining the use of the OAS in the field. These included the development of a filter cartridge and a threaded aluminum cap incorporating a size-selective inlet. The use of an internal filter cartridge eliminated the need for filter contact in the field (during change outs), which reduced the risk of contamination from handling and aided in transport to and from the lab. A threaded aluminum cap sealed the filter cartridge in place and provided a rough inlet to protect against intrusion by small insects. Modifications and additions to the UPAS technology used to create the OAS are depicted in Figure 3-1(left panel); the UPAS is depicted in Figure 3-1(right panel). Numbers and letters shown in Figure 3-1 corresponding to OAS and UPAS components are listed in Table 3.

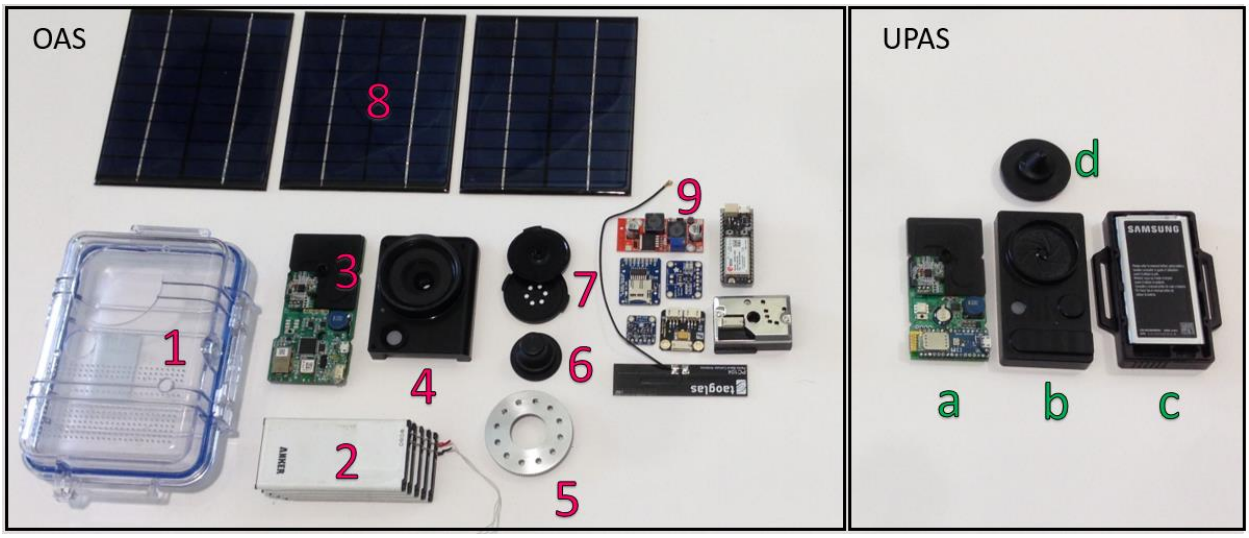

Figure 3-1. OAS evolved from UPAS technology and the various components added, left; UPAS technology, right.

Table 3. OAS and UPAS individual components corresponding with Figure 3-1.

Number	OAS Component
1	Weatherproof enclosure
2	Modified battery pack
3	UPAS circuit board
4	Circuit board housing
5	Threaded aluminum cap
6	Modified size-selective inlet
7	Filter cartridge
8	Solar cells
9	Particle Electron, SMS and antenna, current/voltage meter, Sharp PM sensor, data logger, voltage regulator, meteorological variables sensor
Letter	UPAS Component
A	UPAS circuit board
b	Circuit board housing
c	Battery pack and housing
d	Size-selective inlet

Like the UPAS, the OAS achieved a relatively compact size (17 x 12 x 10 cm), a low weight (888 grams) and quiet operation. The added costs (bill of materials) to convert the UPAS into the OAS totaled $183 for a single unit (Table 1). The inclusion of solar and additional battery power allowed the OAS to be successfully deployed for extended periods of time. The integration of wireless remote communications provides control of the OAS from distant locations and data transmission in real-time. A durable weatherproof enclosure and solid mounting system allowed the OAS to be operated during all months of the year, through strong winds, rain, and snow. The addition of a low-cost sensor allowed for estimation of time-resolved concentrations during a sampling event.

3.2 Power

Power failure probabilities for the month of April, based on Monte Carlo simulations of several OAS configurations, are shown in Figure 3-2. The failure probability is the likelihood the OAS will experience power failure before the conclusion of a given number of consecutive sampling days. As expected, these simulations demonstrate that the OAS run performance is sensitive to both the number of solar and battery cells (Figure 3-2). Based on these simulations, a final design consisting of three solar panels

(0.042m^2 total) and five battery cells (totaling 54 watt-hours of capacity) was chosen. This design maximized performance while also meeting specified design criteria for instrument cost, size, and weight.

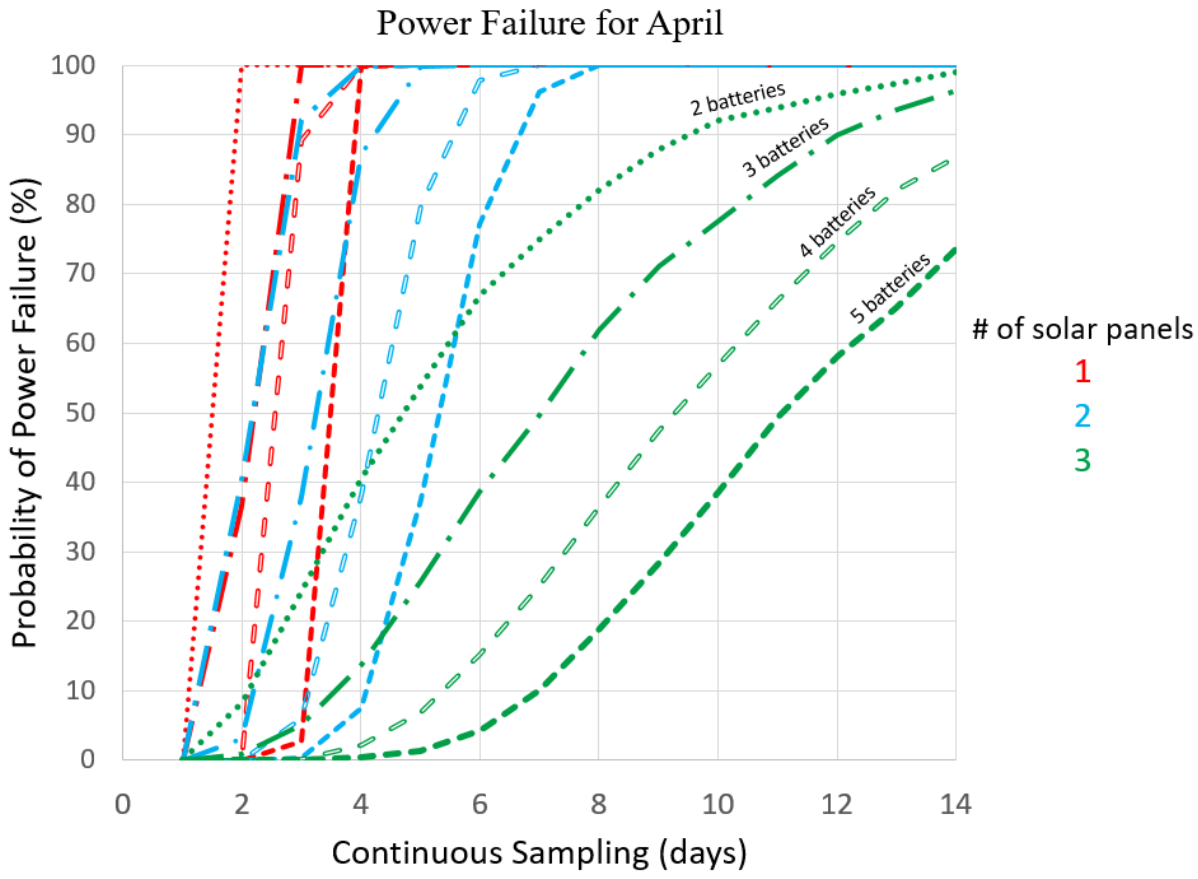

Figure 3-2. Probability of OAS power failure evaluated for various power designs (solar cells, battery capacity) as a function of the number of continuous sampling days. Colors represent the number of solar panels (0.014m^2 each) and line type represents number of Li-ion batteries (10.78 W-hrs. each) included.

Power failure probabilities for the final OAS design with 3 solar cells (0.014m^2 each) and 5 Li-ion batteries (10.78 W-hrs. each) are shown in Figure 3-3. The simulations shown in Figure 3-3 suggest that the OAS can achieve 3 full days of continuous sampling during late Fall and Winter, greater than 4 days in Spring months, and a full week of continuous sampling in Summer. The final OAS power design evaluation of all months is shown in Figure 7-1 located in the appendices. The runtime for the final power

design allows for 2 full days of continuous sampling for all months of the year, regardless of the availability of solar power.

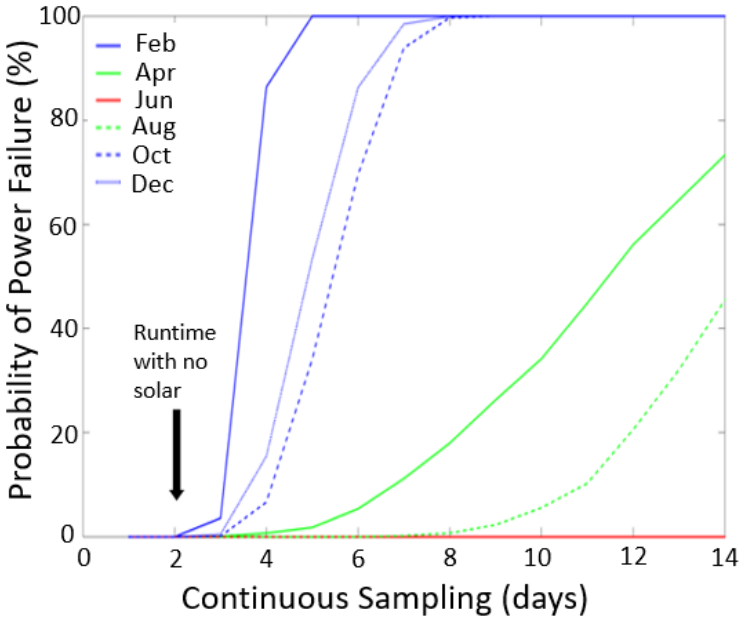

Figure 3-3. Monte Carlo simulation results showing OAS power failure probability for every other month of the year. Axes define number of continuous sampling days and probability of power failure. Colors represent selected months spanning four seasons.

Solar power harvested by the OAS was compared to solar irradiance data for the duration of the prescribed burn sampling near Bayfield Colorado. The ratio of energy collected by OAS to the 24-hour average of solar irradiance striking the solar panels was 6.7 %. The solar energy conversion efficiency of each OAS for all sampling periods while deployed on the prescribed burn is shown in Figure 3-4. Solar irradiance reaching ground level can be absorbed or reflected by fire emissions overhead, reducing the flux of solar energy available for conversion by OAS solar cells. Fire emissions are spatially and temporally variable, which could contribute to differences in irradiance measured by the weather station (at one location) and irradiance observed by each OAS (at other locations). Solar efficiency for samplers in locations below 100 µg/m^3 are represented by black dots and samplers in locations over 100 µg/m^3 are represented by red dots. This labeling scheme was added to mark samplers that may exhibit poor

conversion efficiency due to the presence of smoke. The 6.7% average efficiency was slightly less than the anticipated 7.5% efficiency used in the Monte Carlo model and design phase. Nonetheless, the solar circuit was successful in adding an average of 10 hours runtime to the OAS each day. Contribution of runtime added to each OAS via solar is shown in Figure 7-2 in the appendices section of this document.

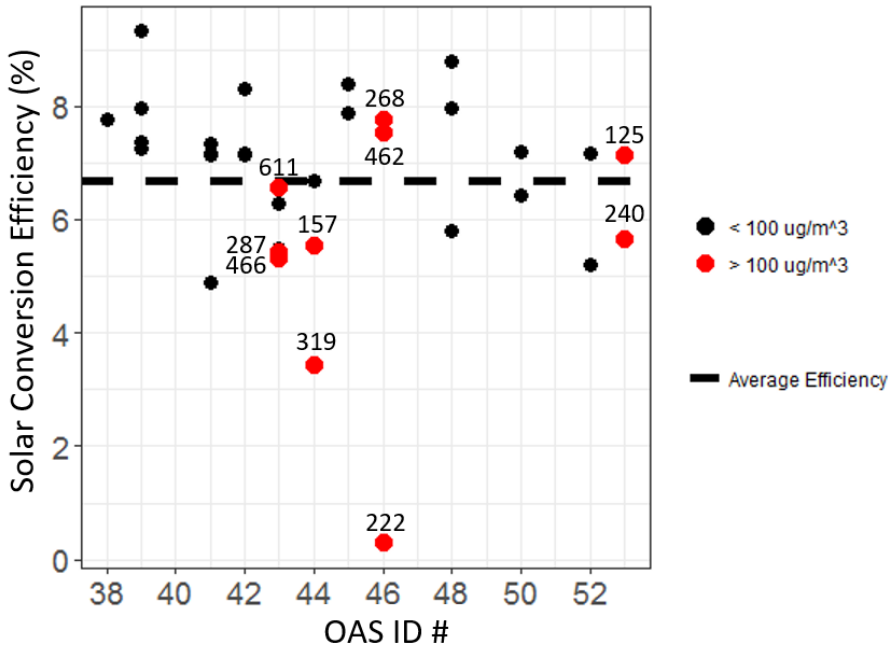

Figure 3-4. OAS solar conversion efficiency during prescribed fire sampling. Colors specify whether sampler was in high or low concentration for the duration of the sampling period. Concentrations over 100 µg/m^3 are labeled. Axes represent solar conversion efficiency and sampler ID number.

Solar irradiance measurements from a single weather station located on Pargin Mountain (at the approximate center of the OAS network) were used to estimate solar efficiency for each OAS device. The OAS monitoring network spanned a linear distance of approximately 26 kilometers. Solar irradiance shielding from smoke can vary significantly over such distances, thus creating possible sources of error in determining an accurate solar conversion efficiency. The rate of solar energy converted by each OAS with respect to time for September 17th, 2016 is shown in Figure 3-5. Irradiance shielding from smoke affected samplers 41, 43, 44, 46, and 53 while samplers 39, 45, and 48 had little obstruction for the duration of the

sampling period. US Forest Service weather observation logs reported clear skies during daylight hours on Sept 17th, 2016, meaning solar irradiance shielding that occurred on this day was likely due to smoke.

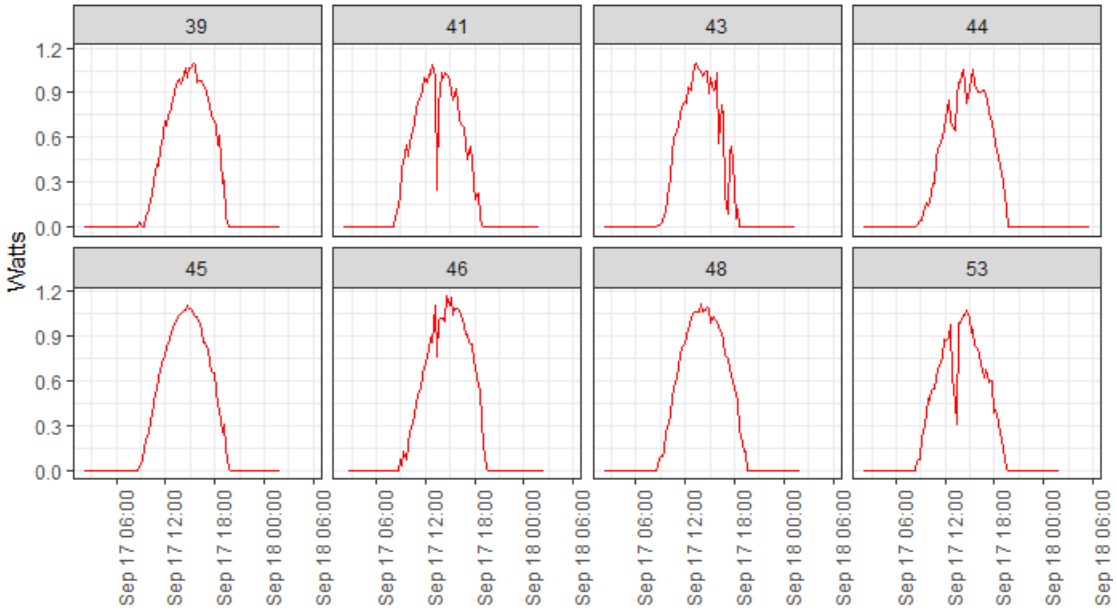

Figure 3-5. Rate of OAS solar power converted as a function of time for Sept 17th 2016. Axis represent rate of solar power harvested and time. Sampler ID numbers are shown at the top of each panel. The x axis represents date and time; the y axis represents solar input power (Watts).

The run performance of each OAS on each prescribed fire deployment is shown in Figure 3-6. Any OAS that operated without issue is shown in green; OAS that experienced a power failure or other technical failure are shown in red and orange, respectively. Failure was defined as sampling for less than the 24-hour goal or if average OAS flow rate was not within 12.5% of specified flow rate (2 L/min). Power consumed by the OAS is strongly dependent on filter loading, which is a function of the sampled aerosol mass concentration. High filter loadings create greater than normal pressure drops across the OAS filter, forcing the pumps to work harder to maintain flow rate. As a result, the OAS consumes more power, which decreases runtime. Eleven of twelve OAS successfully completed the 24-hour sampling period on 9/15/2016. Five OAS fully completed the 24-hour sampling period on 9/18/2016 while 5 experienced power

failure. Depleted from 4 previous 24-hour sampling periods and the high $PM_{2.5}$ concentrations experienced on 9/17/2016, 9/18/2015 saw 5 of the 12 samplers fail due to lack of power.

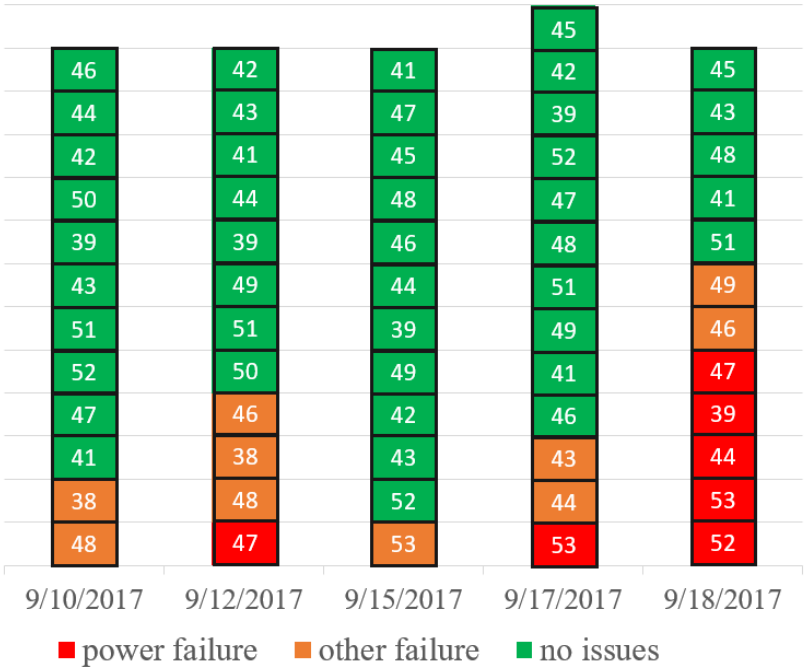

Figure 3-6. The operational status of each OAS at the conclusion of each sampling day. Colors represent failure mode; numbers in each rectangle represent OAS identification number.

Run performance of each OAS was evaluated using the same criteria for the urban deployments. One notable difference from prescribed fire deployments is that the OAS battery packs were exchanged with a fully charged battery pack between each 48-hour sampling period. A minor electrical issue with the OAS circuit board was also resolved prior to urban deployments. All OAS operated without issue for each urban deployment, encountering zero failures of any type.

3.3 Prescribed Fire

Spatial variations in daily (24-hr) $PM_{2.5}$ concentrations measured by the OAS network are depicted in Figure 3-10. Topography played a significant role in creating strong gradients in observed $PM_{2.5}$ concentrations. An early morning photo (Figure 3-7) taken September 18, 2016 from Chimney Rock facing west shows the location of samplers in the OAS network. Smoke from the smoldering fire (red arrows) is

observed flowing down slope into valley bottoms. The phenomenon shown in Figure 3-7 most frequently occurs during late evening and early morning hours when weather conditions favor a stable atmosphere. Smoke dispersion is generally restored or increased, shortly after sunrise when atmospheric stability is upset. An image (Figure 3-8) captured on the morning of Sept 17th from a relay station, 2.4 kilometers northwest of Vance Ranch (location 9) facing east, depicts the location of OAS from a different view point than that of Figure 3-7. On Sept. 17th and Sept. 18th, visible smoke was observed at ground level for as long as 12-14 hours before dissipating. Such events can lead to extremely high $PM_{2.5}$ concentrations. Major concerns resulting from such high concentrations include health hazards for those exposed and visibility concerns along roadways.

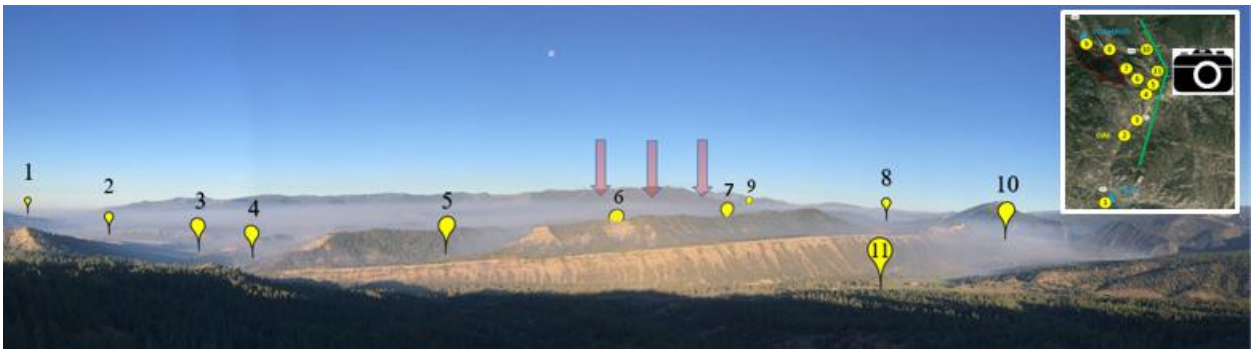

Figure 3-7. View from Chimney Rock, facing west on the morning of Sept. 18, 2016 when smoke is visible in several valleys. (Photo courtesy of Columbine Wildfire Management). OAS locations depicted by yellow markers. Visible smoke is observed around several OAS while other locations appear to be smoke free. Red arrows indicate location of prescribed fire operations.

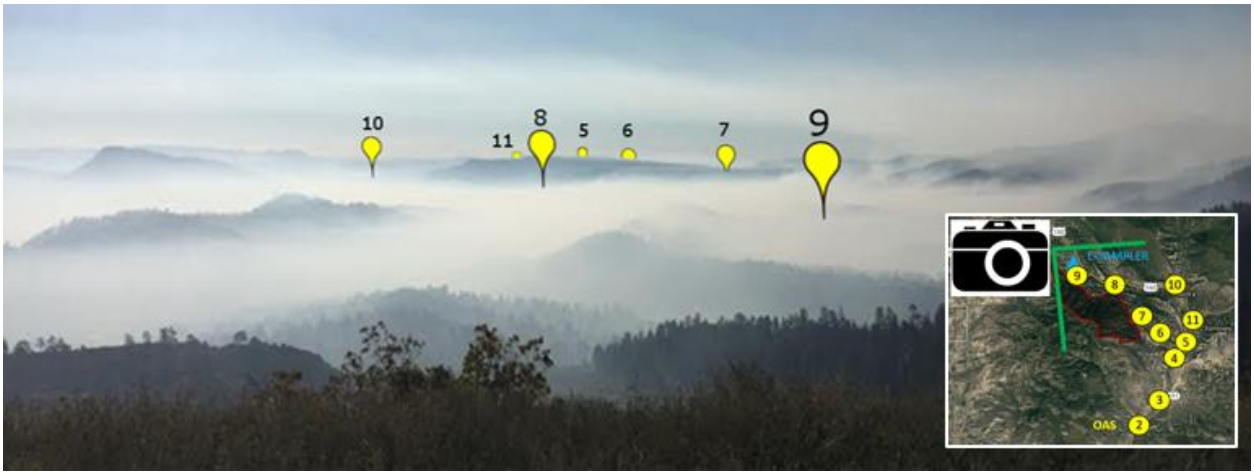

Figure 3-8. Smoke covering valley floors caused by an inversion on the morning of Sept 17th, 2016. Photo taken from relay station 2.4 km northwest of Vance Ranch (location 9) facing east. (Photo courtesy of Columbine Wildfire Management)

The well characterized Pallflex line of filters previously used with UPAS samplers was discontinued: an alternative filter (Tisch PTFE) was selected. Tisch PTFE filters were selected for the prescribed fire sampling because they exhibit a low pressure drop across the filter, and are comprised of hydrophobic Teflon material. The low pressure drop allows the OAS to consume less power while actively sampling. Teflon material is hydrophobic and less susceptible to organic vapor adsorption artifacts than quartz based filters [58, 59].

Prescribed fire sampling results suggested a low collection efficiency for combustion sized aerosol (< 1µm diameter) using the Tisch PTFE filters. Lab tests confirmed the low collection efficiency. Tisch PTFE filter collection efficiency as a function of particle size is shown in Figure 3-9. The average collection efficiency is depicted by a black line; grey shading represents ± 1 standard deviation. The red plot represents a hypothetical aerosol mass distribution produced by prescribed fire (derived from [26]). Applying the laboratory-derived filter collection efficiency to the estimated prescribed fire distribution results in the green shaded area representing the aerosol mass distribution collected by the Tisch filter. These filters had an estimated mass collection efficiency of 66.7% and a count collection efficiency of 68.2%. All plots

containing mass concentration data in the results section of this document have been corrected for filter collection efficiency.

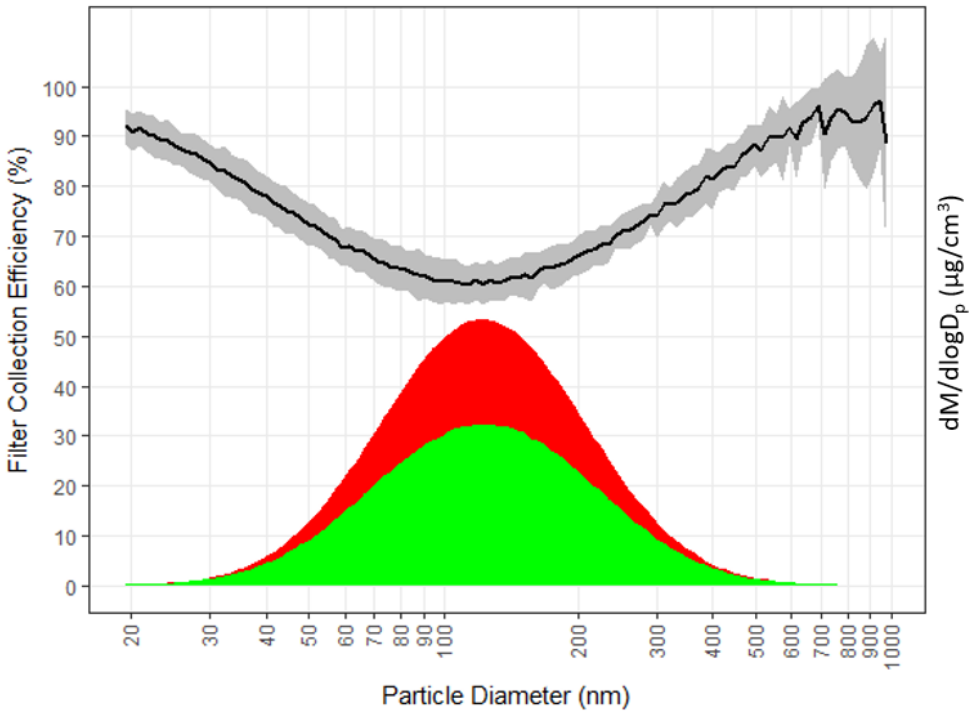

Figure 3-9. Collection efficiency of 37mm Tisch PTFE filters (2L/min flow) with respect to particle mobility diameter and mass distribution of particles (red) and mass distribution collected by the filters (green). Primary vertical axis represents filter collection efficiency; secondary vertical axis represents actual and measured particle size distributions (by mass). Horizontal axis is particle size.

Data mapping and interpolation techniques were used to investigate the spatial and temporal evolution of ground-level $PM_{2.5}$ concentrations from September 12th through September 18th, 2016. Maps illustrating interpolated mass concentrations for each 24-hour field sampling period are shown in Figure 3-10. Data from September 10th, 12th, and 18th are shown; data from September 15th, and 17th are shown in Figure 7-3 of the appendices. PM mass concentrations are represented by color, depicting coarse concentration gradients across space. Colored regions reflect the following concentration ranges: green, concentrations at or below the NAAQS annual $PM_{2.5}$ limit (15µg/m^3); yellow, concentrations falling between the annual limit

(15µg/m^3) and the NAAQS 24-hour $PM_{2.5}$ limit (35µg/m^3); orange, concentrations falling between the 24-hour NAAQS limit (35µg/m^3) and 100µg/m^3; and red, concentrations in excess of 100 µg/m^3. Average, 24-hr mass concentrations greater than 100µg/m^3 (red) are labeled next to an individual sampling site on the map. Wind speed and direction data during each 24-hour sampling period are illustrated by a wind rose located to the right of each map.

Some samplers encountered power failure before completing the entire sampling period; the results from those samplers are still potentially useful in estimating mass concentrations, as nearly all power failures were the result of high particulate mass loadings on the filters. These concentrations were calculated by letting the mass accumulated on the filters represent the entire 24-hour sampling period to estimate a lower bound of average mass concentration for that site and sampling day. Prior to the 9/18/2016 sampling period, each OAS that encountered power failure measured a 24-hour average mass concentration in excess of 100µg/m^3.

On Sept 10th (Figure 3-10a), winds were predominantly from a northerly direction at around 7 km/hr. Aerosol concentrations were at or below NAAQS 24-hour average acceptable limit in areas furthest form the fire while areas of closer proximity were between 35 and 100 µg/m^3. Locations north of the fire observed high concentrations. On Sept 12th (Figure 3-10b), winds were predominantly from the NW to N direction at around 6 km/hr. Concentrations were at or below NAAQS 24-hour limit in most areas. Locations adjacent to the fire as well as downwind and downslope observed high concentrations. On Sept 18th (Figure 3-10c), winds were predominantly from a northerly direction at around 8 km/hr. Concentrations were inconsistent across sampling locations, demonstrating the heterogeneity of emissions that may exist near a fire.

In most cases, the strong concentration gradients depicted in Figure 3-10 are the result of weather conditions in combination with geographical features of the surrounding landscape. The concentration map shown in Figure 7-1a is from time frame September 17, 1:00 AM through September 18, 1:00 AM. Smoke blanketing valley floors from an inversion is shown in Figure 3-8; this smoke contributed to the high concentrations sampled September 17.

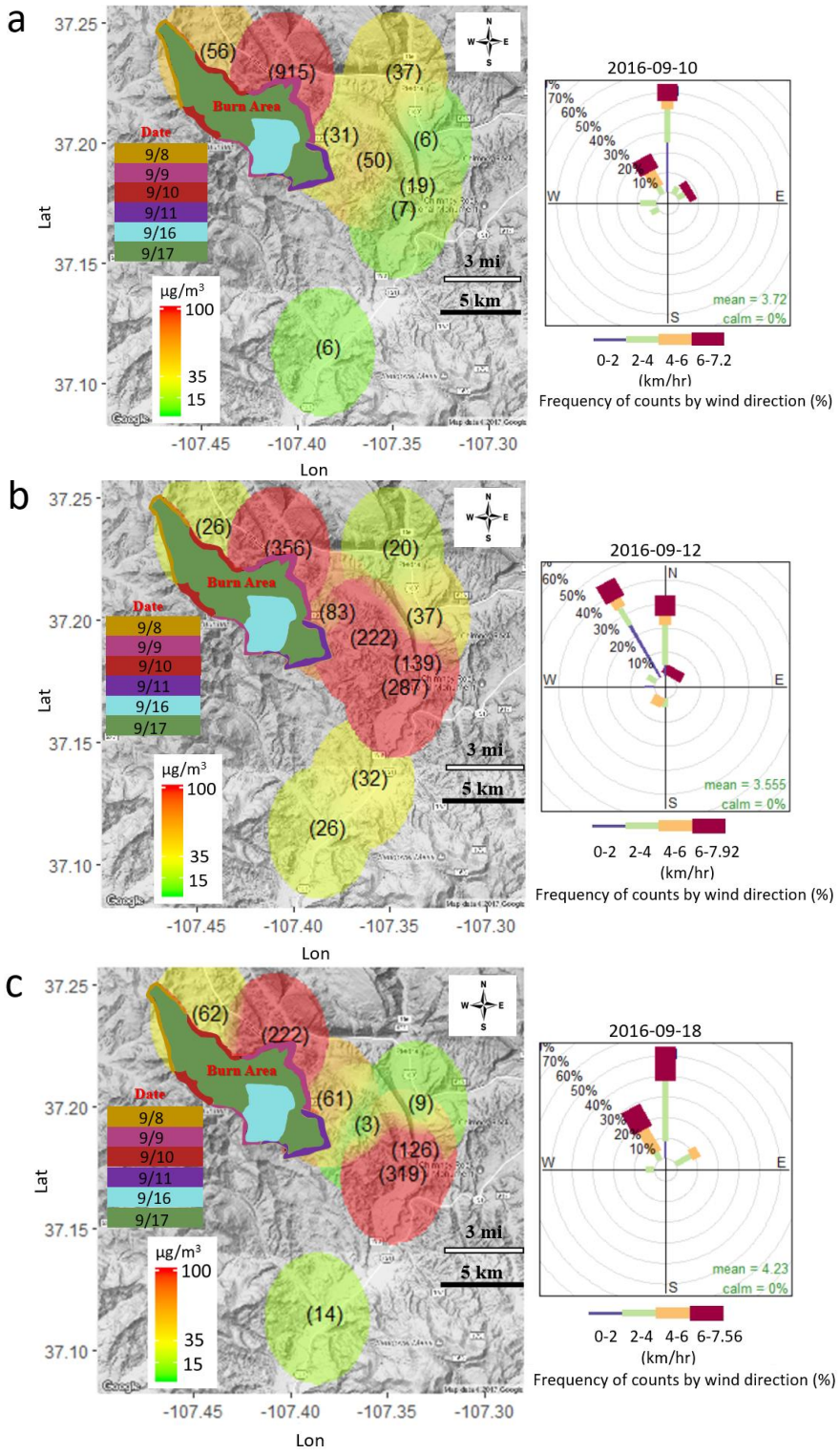

Figure 3-10. Maps illustrating spatial concentration gradients and the temporal evolution of fire emissions for (a) Sept 10th, (b) Sept 12th, and (c) Sept 18th of 2016.

PM concentrations measured across the OAS network are shown in Figure 3-11 for all sampling days. US Forest Service air quality monitoring equipment (E-SAMPLER and E-BAM) measurements are represented in Figure 3-11 by red and turquoise lines, respectively. Concentrations are represented in comparison to NAAQS 24-hour PM acceptable limit (35µg/m^3). The OAS network captured a wide range of $PM_{2.5}$ concentrations; this range was reflected by the USFS monitors on only two of the five deployments. Thus, even with only 13 monitors, the OAS provided a more spatially comprehensive assessment of smoke impact in the immediate vicinity of the prescribed burn. One key advantage of the OAS, in this regard, is that monitoring can take place in remote areas that lack line power (necessary to operate equipment like the E-BAM and E-SAMPLER).

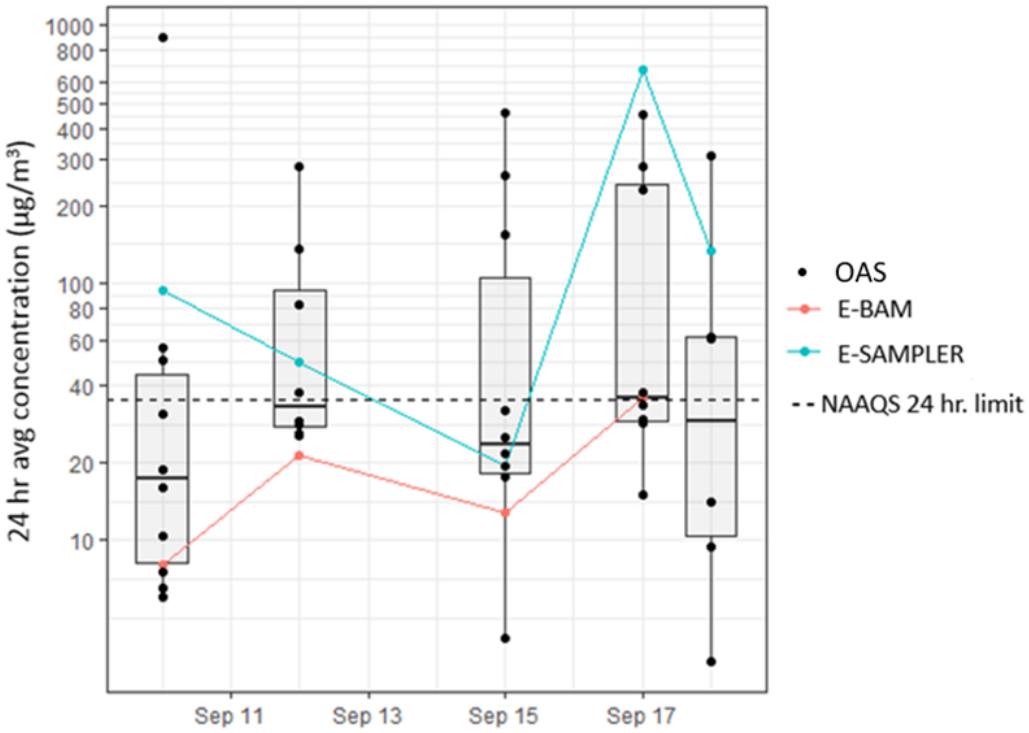

Figure 3-11. Prescribed fire summary of air quality at all locations for all dates sampled by both OAS and Forest Service equipment (E-BAM and E-SAMPLER).

A performance comparison between the OAS and E-BAM (co-located at Arboles Fire Station, location 1) is shown in Figure 3-12. The E-BAM measures PM mass concentrations by using Beta attenuation and performs well in comparison to FRM monitors [31]. A simple linear regression of the E-BAM and OAS gives a slope of 0.97 and an intercept of -4.9 µg/m^3. The room mean square error (RMSE) of the regression is 2.5 µg/m^3; coefficient of determination (R^2) is 0.92.

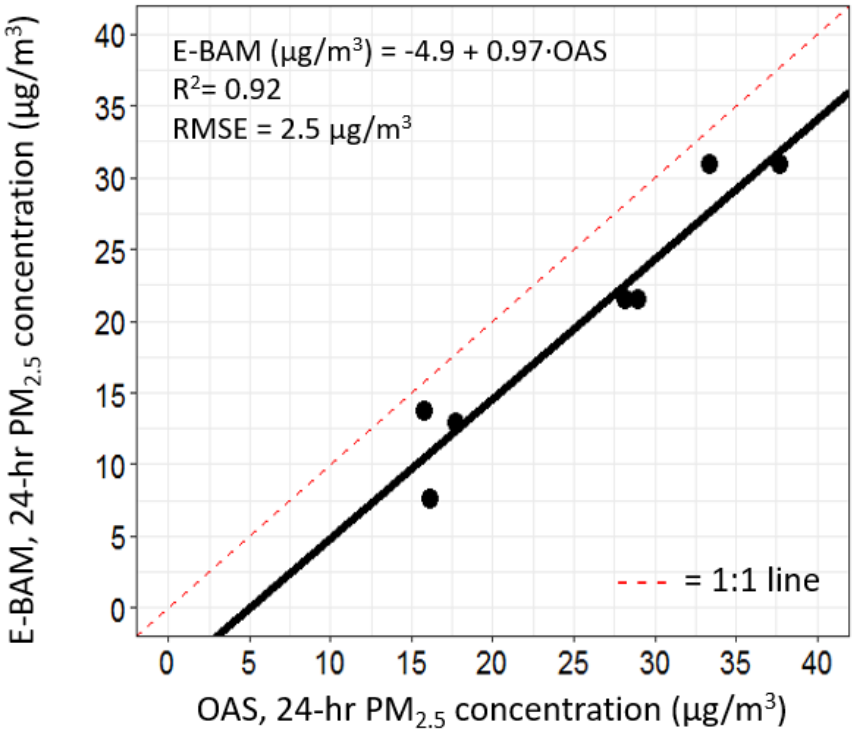

Figure 3-12. Performance of the Outdoor Aerosol Sampler relative to an E-BAM federal equivalent Monitor (meets US-EPA requirements for Class III designation for $PM_{2.5}$).

3.4 Urban Deployment

The performance of the OAS relative to EPA federal equivalent method (FEM) sampler (Grimm model 180) is shown in Figure 3-13. An errors-in-variables model (Deming regression) was used to estimate a linear fit between the OAS and FEM instruments. Deming regression accounts for errors in both the x and y axis by minimizing the perpendicular distance between the best fit line and data points. Assuming the

errors of the Grimm and OAS to be independent and normally distributed, the best fit line gave a slope of 0.93, an intercept of -0.7 µg/m^3, a correlation coefficient (Pearson's R) of 0.71 and a coefficient of determination (R^2) of 0.5. The RMSE of the Deming regression is 1.4 µg/m^3.

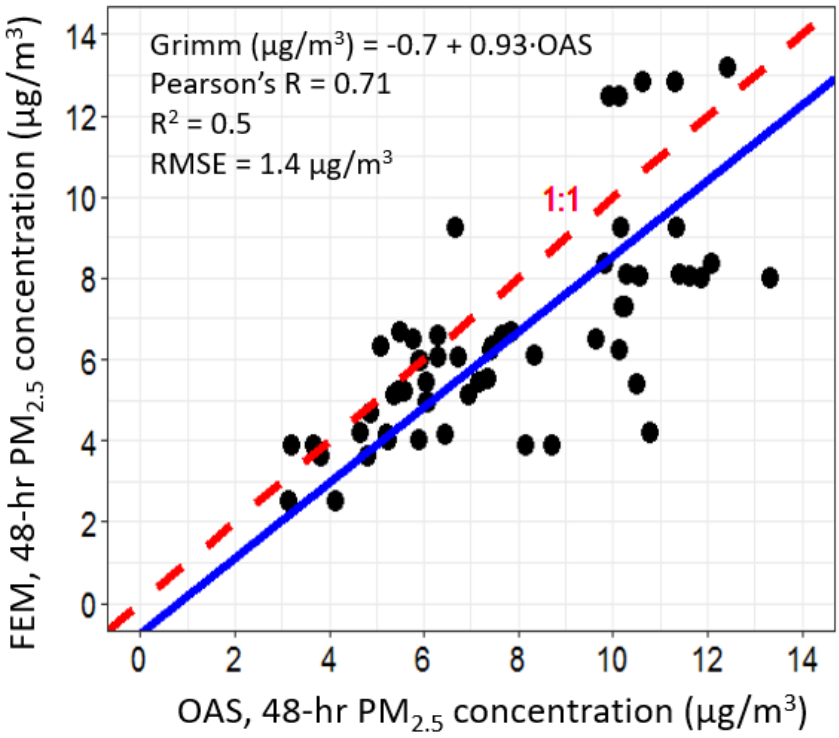

Figure 3-13. OAS relative to EPA federal reference method equivalent (FEM) sampler, Grimm model 180.

The Grimm 180 determines aerosol concentration by light scattering [60]. The amount of light scatted by the aerosol (Mie scattering intensity) depends on particle size, refractive index, shape, and wavelength of incident light [37]. Mass concentrations reported by the Grimm 180 are calculated from the amount of light scattered by each particle and an assumed aerosol density. The OAS measures aerosol mass concentration by physically depositing $PM_{2.5}$ onto a filter, which is then weighed. The gain in filter mass and volume of air sampled are then used to back calculate mass concentration. The Grimm and OAS measurement techniques are fundamentally different. A straightforward comparison between the two

methods is difficult to make. Sources of error are difficult to establish because factors like aerosol density, and relative humidity impacts each measurement method differently.

Grimm instruments are calibrated to urban aerosol and assume a constant density for all particles sampled [60]. The constant density assumption does not allow the Grimm to correct for particles of varying density. The Grimm has been observed to under sample FEM monitor BAM (MetOne Instruments) and FRM filter-based sampler Partisol (FRM2000, Thermo Fisher Scientific, Waltham, MA, USA) in an outdoor setting by as much as %30 percent in some instances [61, 62].

Deming regression was used for urban sampling OAS performance comparison to Grimm samplers in order to relax the assumption of the Grimm being an exact reference. A simple linear model was used in the prescribed fire sampling performance comparison to the E-BAM. The E-BAM was considered to be an accurate reference for mass concentration; therefore, no E-BAM error is considered and a Deming regression is not necessary.

3.5 Real-time PM Sensing

Mass concentration measurements from the Sharp sensor proved too inconsistent to be used as a trigger mechanism. This real-time sensor suffered from temperature dependence, drift and precision issues as well as previously documented problems associated with accurate PM measurement by means of light scattering. These problems include signal loss at particle sizes below 1 micron [37], humidity effects [38], variation of Mie scattering intensity as a function of size and refractive index [63], and lack of ability to distinguish different particle densities. Fire emissions are primarily composed of sub-micron particles [64], making signal loss at submicron particle sizes a very important issue when sampling such emissions. A change in fire emission particle size distribution below the lowest detectable particle size will go unmeasured.

The relationship of output signal (voltage) from the Sharp sensor as a function of time while in an outdoor setting is shown in Figure 3-14. At 95 hours, the sensors were repositioned. A large change in sensor output (gain and offset) is observed due to the disturbance, demonstrating the sensitivity of the low-cost sensor to physical perturbations. This change in sensor response due to the repositioning was not consistent across all sensors. Drift over time was also observed and was not consistent across all samplers.

Drift may result from PM depositing on the Sharp's internal optics over time. Rate of drift is expected to increase with PM concentrations. The strongly correlated linear relationship between sensor output and temperature (a function of diurnal cycling) is depicted in Figure 3-15a. The Sharp's drift and influence from meteorological variables has been documented by various studies [65, 66].

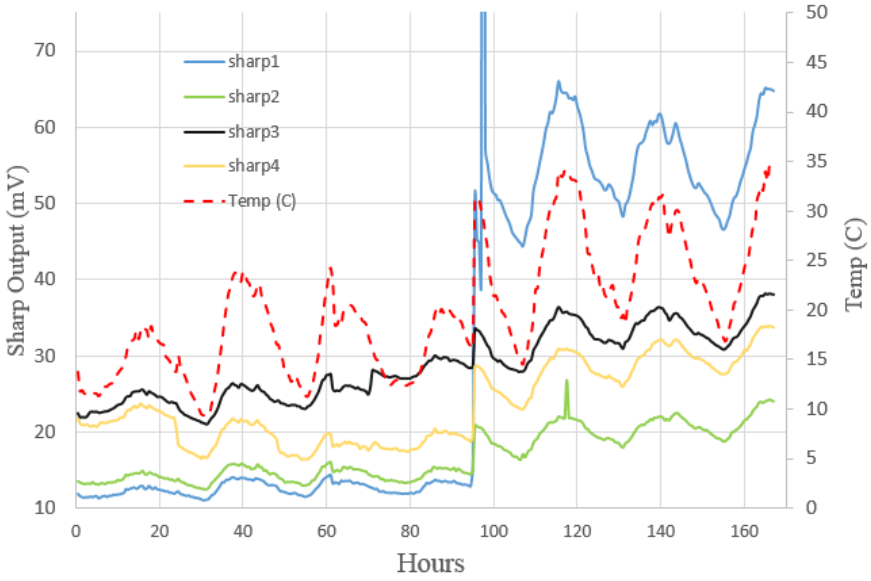

Figure 3-14. Sharp GP2Y1023AU0F output voltage with respect to temperature and time while sampling outdoors.

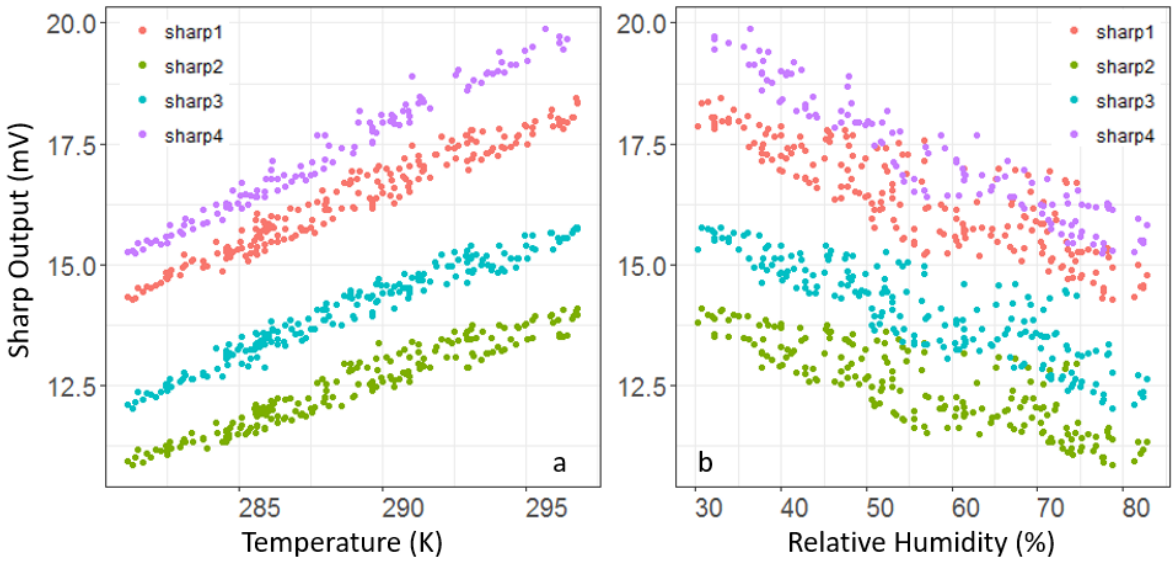

Figure 3-15. Sharps output correlation with a.) temperature and b.) humidity.

A multivariate polynomial regression (MFP package in R) model was developed to relate the response of the Sharp instrument to temperature and humidity variations. The temperature and humidity inputs to the model ranged from 281 K to 295K and 12% to 87%, respectively. Equation 9 describes the adjustment applied to Sharp measurements using meteorological variable manipulation to obtain a more accurate mass concentration measurement;

$$Corrected\ Sharp = Sharp + 59.037\left(\frac{RH}{100}\right)^3 + 35.651\left(\frac{T(°K)}{100}\right) - 98.631 \qquad (9),$$

where RH is relative humidity (%), and T(°K) is temperature in Kelvin and the output units are in µg/m^3.

The overall fit of Sharp concentration measurements (4 Sharps, 95 hours), adjusted for meteorological variables, to measurements taken by a co-located DustTrak DRX (TSI Inc., Shoreview, MN, USA) is shown in Figure 3-16. The fit has a RMSE of 9.9 µg/m^3 and R^2 of 0.36.

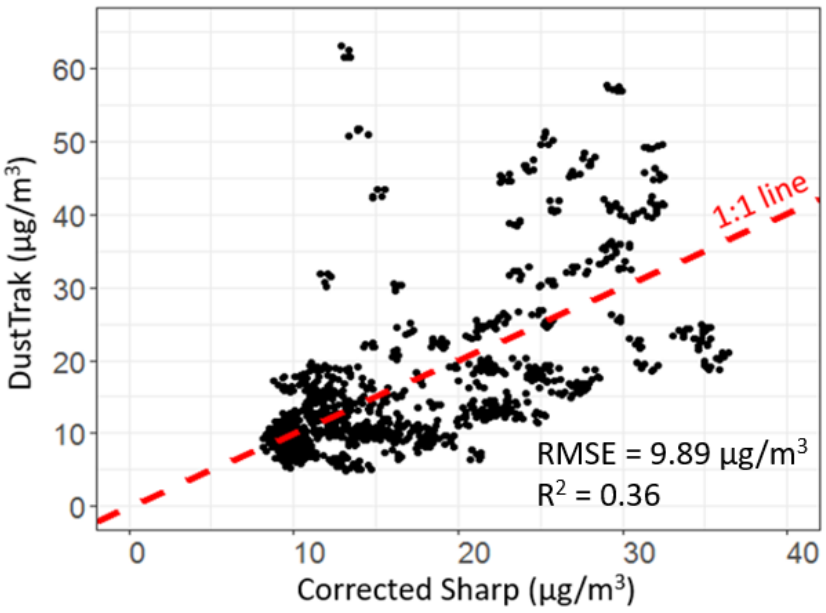

Figure 3-16. Concentration measurements (averaged on a 30-minute interval) of low-cost PM sensor (Sharp) corrected for meteorological variables (temperature and humidity) plotted against co-located DustTrak.

Equation 9 was used to correct Sharp measurements from the field. The majority of meteorological variables measured in the field used to correct the Sharp fell within the range used in developing the correction equation. However, a small percentage of data (approximately 15%) was outside the model range; Equation 9 was extrapolated for these data. The inconsistent drift issues and high disturbance sensitivity of the Sharp were not accounted for in this model. Due to these issues, a no-concentration threshold for Sharp output cannot be determined unless a calibration is done before each sampling period, which is not practical for remote field sampling. Further, a rate of drift must still be assumed for each device. Time-resolved measurements from the sharp were derived by means of in-situ calibration (OAS gravimetric measurements). Time-resolved mass concentration measurements from the real-time optical sensor for (A) September 12th (location 7) and (B) September 15th (location 6) are shown in Figure 3-17. The black line represents measurements with no meteorological variables correction applied, while the red line denotes the mass concentration measurement of the Sharp adjusted for meteorological variables.

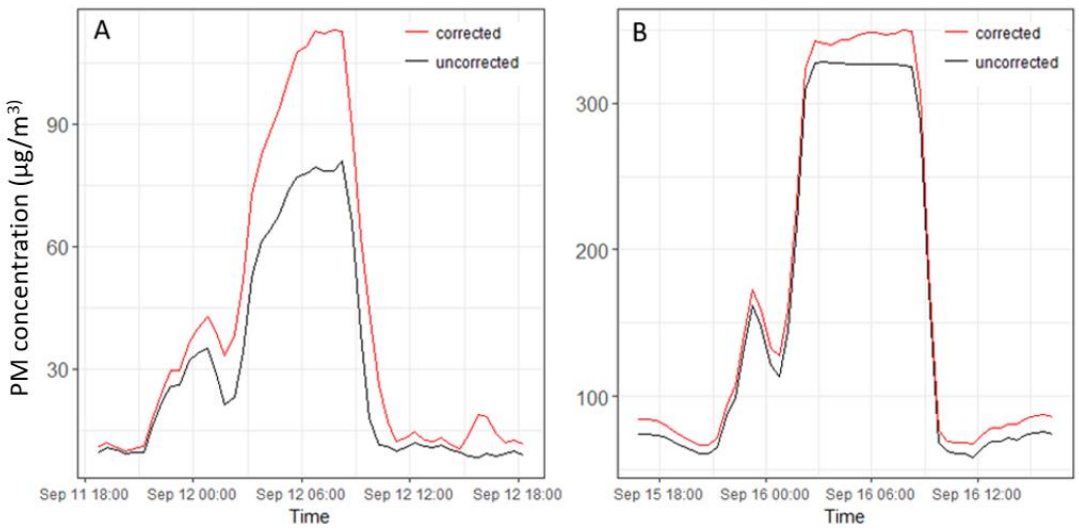

Figure 3-17. Particulate mass measurements from the low-cost real-time sensor (Sharp GP2Y1010AU0F) for (A) September 12th, location 7; (B) September, 15th, location 6.

Despite the real-time sensor being of little use as a trigger mechanism, the OAS demonstrated the capability of detecting large smoke plumes. The OAS's remote communications and controllability through SMS technology enable: wireless transmission of smoke plume detection alerts; reporting of meteorological variables and real-time sensor readings directly to the user's phone (or any device with an internet connection); and remote OAS pump toggling.

CHAPTER 4. CONCLUSIONS

Reference instruments used to assess outdoor air quality tend to be expensive and bulky. This project developed and tested an Outdoor Aerosol Sampler (OAS) that is compact, weatherproof, independently powered, and designed to provide reference-quality measurements of $PM_{2.5}$. Results from a Monte Carlo simulation, assuming an overall solar circuit efficiency of 7.5%, determined that three solar cells (0.014m^2 each) and 50 watt-hours of Li-ion battery capacity (five 10.78 Watt-hr. batteries) would provide enough energy to independently power the OAS. The simulation suggests the Outdoor Aerosol Sampler (OAS) is capable of 1-2 week-long outdoor deployments, with periodic downtime for solar recharging in non-summer months.

Numerous OAS were deployed on a large prescribed fire in southern Colorado to evaluate its effectiveness as a smoke monitoring tool. The OAS network worked well as a smoke monitoring tool, providing spatially resolved measurements in regions where sampling with current state-of-the-art equipment was not possible. Interpolated concentration maps, generated from prescribed fire sampling results, depict aerosol concentrations near the fire ranging from less than 15µg/m^3 to over 500µg/m^3 across the sampling campaign. Strong concentration gradients were observed and likely present due to topographical features (e.g. mountain ridges) and diurnal weather patterns. The prescribed fire field sampling average solar conversion efficiency of 6.7% was slightly less than the 7.5% efficiency input to the Monte Carlo simulation. Nonetheless, the solar circuit performed as expected and was successful in adding an average of 11 hours runtime to the OAS during a 24 hour period. The real time optical sensor (Sharp GP2Y1023AU0F) integrated with the OAS was determined to be unreliable for measuring PM in an outdoor setting accurately enough to serve as a trigger mechanism. The sensor was affected by meteorological variables and inconsistent drift patterns. These issues precluded the ability to establish a baseline concentration (without in-situ calibration) prior to each deployment, which is limits the practicality of the Sharp sensor for remote outdoor sampling. However, applying a correction equation for

meteorological variables and using OAS gravimetric post sampling results for calibration, qualitative time-resolved measurements were achieved with the Sharp sensors.

Urban sampling OAS performance was relatively accurate but imprecise in comparison to a FEM sampler (Grimm model 180, nephelometer). A Deming regression of the OAS and FEM yielded: a slope of 0.93, an intercept of -0.7µg/m^3, a Pearson correlation coefficient of 0.71, and a root mean square error of 1.4 µ/m^3.

The affordability, independent power capability, and compactness of the OAS provide a practical solution to effectively monitoring smoke from a prescribed burn or wildfire event. A successful demonstration of a low-cost sensor network represents a first step towards providing burn managers, state and federal agencies, and concerned citizens with a better understanding of fire smoke emissions and resulting exposures. The OAS is not limited to fire events only and may be used for many other applications of outdoor air quality monitoring.

Epidemiology studies depend on accurate exposure estimates to minimize exposure misclassification. Land-use regression models are a common approach to visualize the spatial distribution of pollution concentrations in expose assessments. These models rely on ground based air quality measurements. Available measurements are generally sparse due to the high cost of sampling equipment and necessary personnel. At nearly 1/20th the cost of current state-of-the-art field monitoring equipment, the OAS can be affordably deployed and operated in large quantities. Air quality data at more locations would enhance the accuracy of land-use regression models, yielding a more comprehensive estimate of exposure and health hazards.

CHAPTER 5. LIMITATIONS AND FUTURE WORK

The Monte Carlo simulation was based on data from Fort Collins, Colorado between 2011 and 2015. Weather patterns, a large driver of solar irradiance available, are expected to vary by region. The accuracy of simulated power failure probabilities is expected to decrease when OAS are deployed outside of Colorado's Front Range. This decrease in failure probability accuracy inhibits OAS deployment length estimation and adds an additional challenge to operating an OAS network with minimum failures.

The simulation calculated power budget and power failure on a daily basis (as opposed to hourly); thus, the temporal resolution of the model was limited. Days modeled were randomly selected (not consecutive) within the specified month for any of the 4 years. Random selection of days can attenuate the effect of large weather systems, which may have a more significant impact on OAS runtime. The OAS power consumption was also assumed to be constant at 0.7 Watts. This assumption did not allow the simulation to account for high filter loadings and the associated increased OAS power consumption. The Monte Carlo simulation could be improved by evaluating power failure hourly and accounting for a range of filter loadings.

Prescribed fire sampling demonstrated premature OAS power failure as a result of high mass loadings on filters. The results from those samplers are limited to a lower bound of average mass concentration for that site and sampling day. Aerosol concentration largely determines OAS runtime. Runtime is reduced when sampling extremely high concentrations (i.e., > 100 $\mu g/m^3$).

The thirteen OAS samplers deployed in a network on the prescribed fire captured high concentration gradients resulting from smoke. Actual gradients may have been even stronger than what was measured. One method of improving the spatial resolution of the network would be to deploy more OAS units. However, only a certain number of OAS units (approximately 15) can still be feasibly deployed for such a study by a single person.

Filter mass collection efficiencies were derived from chamber testing. Collection efficiency calculations assumed the particles used in the chamber testing had the same shape (spherical) and effective

density as the actual prescribed fire aerosol. A resource quantifying the sphericity of particles generated from biomass burning can be found at [67]. Particles sizes measured in the chamber during testing were classified by electrical mobility diameter. The mobility diameter was assumed to be equal to the volume diameter for the efficiency calculations since particle shape was assumed to be spherical. Filter collection efficiency has been found to increase with filter loading [68]. The mass collection efficiency of a clean Tisch filter was considered to be constant when correcting prescribed fire filter mass accumulated for collection efficiency.

A hindrance of the remote communications method used is the limited availability of the Particle hosted web page. The page is only available while the Particle is online, resulting in increased power consumption if communication is to be maintained at all times. Another issue is the execution frequency permitted by Google Scripts. Google Scripts is a free service; however, execution frequency limits data collection to once per hour. A possible solution addressing the limited availability of the Particle web page would be the use of an interrupt queue. This prompt would significantly reduce server time and power consumption. A personal server designed for OAS communication would alleviate issues associated with data collection frequency and simplify data archiving.

The Sharp suffered from unpredictable drift issues, rendering the real-time measurements unreliable until post sampling calibration could be applied to extract time-resolved measurements. Possible OAS improvements include replacing the real-time sensor (Sharp) with a more reliable low-cost sensor. Low cost $PM_{2.5}$ optical sensing technology is an active area of research and development. An accurate, reliable low-cost sensor would enable the OAS to monitor air quality while remaining in an idle state. Utilizing the low-cost sensor as a trigger mechanism (as originally intended) would allow an OAS network to serve as an early warning tool by detecting and tracking emissions in real time.

Comparing OAS performance relative to Grimm nephelometers demonstrated accurate but imprecise agreement. The Grimm has well documented issues and is known to be erroneous in aerosol mass measurement compared with other FRM methods [61, 69]. An additional performance evaluation of the

OAS is planned for the near future. OAS will be co-located with FRM samplers to compare OAS mass concentrations to a gravimetrically determined FRM monitor mass concentrations.

REFERENCES

1. Willeke, K. and K.T. Whitby, *Atmospheric aerosols: size distribution interpretation.* Journal of the Air Pollution Control Association, 1975. 25(5): p. 529-534.

2. Lighty, J.S., J.M. Veranth, and A.F. Sarofim, *Combustion aerosols: factors governing their size and composition and implications to human health.* Journal of the Air & Waste Management Association, 2000. 50(9): p. 1565-1618.

3. Silva, R.A., et al., *Global premature mortality due to anthropogenic outdoor air pollution and the contribution of past climate change.* Environmental Research Letters, 2013. 8(3): p. 034005.

4. Lelieveld, J., et al., *The contribution of outdoor air pollution sources to premature mortality on a global scale.* Nature, 2015. 525(7569): p. 367-371.

5. Zanobetti, A., et al., *Fine particulate air pollution and its components in association with cause-specific emergency admissions.* Environmental Health, 2009. 8(1): p. 58.

6. Dominici, F., et al., *Fine particulate air pollution and hospital admission for cardiovascular and respiratory diseases.* Jama, 2006. 295(10): p. 1127-1134.

7. Pope III, C.A., et al., *Lung cancer, cardiopulmonary mortality, and long-term exposure to fine particulate air pollution.* Jama, 2002. 287(9): p. 1132-1141.

8. *Clean Air Act Overview*. [cited 2017 4/12]; Available from: https://www.epa.gov/clean-air-act-overview/evolution-clean-air-act.

9. *Particulate Matter Trends*. [cited 2017 4/12]; Available from: https://www.epa.gov/air-trends/particulate-matter-pm25-trends.

10. *Air Emissions Inventories*. [cited 2017; Available from: https://www.epa.gov/air-emissions-inventories/2011-national-emissions-inventory-nei-data.

11. Cohen, A.J., et al., *The global burden of disease due to outdoor air pollution.* Journal of Toxicology and Environmental Health, Part A, 2005. 68(13-14): p. 1301-1307.

12. Gan, W.Q., et al., *Associations of ambient air pollution with chronic obstructive pulmonary disease hospitalization and mortality.* American journal of respiratory and critical care medicine, 2013. 187(7): p. 721-727.

13. Atkinson, R., et al., *Long-term exposure to outdoor air pollution and the incidence of chronic obstructive pulmonary disease in a national English cohort.* Occupational and environmental medicine, 2014: p. oemed-2014-102266.

14. Brook, R.D., et al., *Air pollution and cardiovascular disease.* Circulation, 2004. 109(21): p. 2655-2671.

15. Pope, C.A., et al., *Cardiovascular mortality and long-term exposure to particulate air pollution.* Circulation, 2004. 109(1): p. 71-77.

16. Clark, M.L., et al., *Impact of a cleaner-burning cookstove intervention on blood pressure in Nicaraguan women.* Indoor Air, 2013. 23(2): p. 105-114.

17. Urbanski, S.P., W.M. Hao, and S. Baker, *Chemical composition of wildland fire emissions.* Developments in Environmental Science, 2008. 8: p. 79-107.

18. Westerling, A.L., et al., *Warming and earlier spring increase western US forest wildfire activity.* science, 2006. 313(5789): p. 940-943.

19. DeBano, L.F., D.G. Neary, and P.F. Ffolliott, *Fire effects on ecosystems*. 1998: John Wiley & Sons.
20. Flannigan, M.D., B.J. Stocks, and B. Wotton, *Climate change and forest fires.* Science of the total environment, 2000. 262(3): p. 221-229.

21. Yue, X., et al., *Ensemble projections of wildfire activity and carbonaceous aerosol concentrations over the western United States in the mid-21st century.* Atmospheric Environment, 2013. 77: p. 767-780.

22. Spracklen, D.V., et al., *Impacts of climate change from 2000 to 2050 on wildfire activity and carbonaceous aerosol concentrations in the western United States.* Journal of Geophysical Research: Atmospheres, 2009. 114(D20).

23. *National Interagency Fire Center, Wildland*.

24. *National Interagency Fire Center, Prescribed*

25. *Interim Air Quality Policy on Wildland and Prescribed Burns*, E.P. Agency, Editor. 1998.

26. Chakrabarty, R.K., et al., *Emissions from the laboratory combustion of wildland fuels: Particle morphology and size.* Journal of Geophysical Research: Atmospheres, 2006. 111(D7).

27. Sakamoto, K.M., et al., *The evolution of biomass-burning aerosol size distributions due to coagulation: dependence on fire and meteorological details and parameterization.* Atmospheric Chemistry and Physics, 2016. 16(12): p. 7709-7724.

28. Hardy, C.C., et al., *Smoke Management Guide for Prescribed and Wildland Fire*. 2001, National Wildfire Corporation Group.

29. Mott, J.A., et al., *Wildland forest fire smoke: health effects and intervention evaluation, Hoopa, California, 1999.* Western Journal of Medicine, 2002. 176(3): p. 157.

30. Makri, A. and N.I. Stilianakis, *Vulnerability to air pollution health effects.* International journal of hygiene and environmental health, 2008. 211(3): p. 326-336.

31. *Smoke Particulate Monitors: 2006 Update*, U. USDA, Editor.

32. *Ambient Particulat Monitoring, Thermo Fisher Scientific*. Available from: https://www.thermofisher.com/us/en/home/industrial/environmental/air-quality-analysis/ambient-particulate-monitoring.html.

33. *Air Quality Monitors, Met One Instruments*. [cited 2017; Available from: http://www.metone.com/products/air-quality-monitors/.

34. Hardy, C.C., et al., *Smoke management guide for prescribed and wildland fire: 2001 edition.* 2001.

35. *LIST OF DESIGNATED REFERENCE AND EQUIVALENT METHODS*. 2016 December 17; Available from: https://www3.epa.gov/ttn/amtic/files/ambient/criteria/AMTIC%20List%20Dec%202016-2.pdf.

36. *Air Quality System (AQS)*, U.S.E.P. Agency, Editor.

37. Hinds, W.C., *Aerosol technology: properties, behavior, and measurement of airborne particles*. 2012: John Wiley & Sons.

38. Chakrabarti, B., et al., *Performance evaluation of the active-flow personal DataRAM PM2.5 mass monitor (Thermo Anderson pDR-1200) designed for continuous personal exposure measurements.* Atmospheric Environment, 2004. 38(20): p. 3329-3340.

39. Eiseman, E., *Monitoring for Fine Particulate Matter*. Critical Technologies Institute, RAND.

40. Hand, W.C.M.J.L., *Cpmparisons Between Continuous and Integrated Mass Measurements*, C.I.f.R.i.t. Atmosphere and C.S. University, Editors. 2013.

41. *Air Quality System Data Mart [internet database]* 2016 [cited 2016 3/5/2016]; Available from: https://www.epa.gov/airdata.

42. Liu, Y., et al., *Estimating ground-level PM2. 5 in the eastern United States using satellite remote sensing.* Environmental science & technology, 2005. 39(9): p. 3269-3278.

43. Lassman, W., *Blending Model Output with satellite-based and in-situ observations to produce high-resolution estimates of population exposure to wildfire smoke*. 2017, Colorado State University. Libraries.

44. Patel, S., et al., *Spatio-temporal measurement of indoor particulate matter concentrations using a wireless network of low-cost sensors in households using solid fuels.* Environmental Research, 2017. 152: p. 59-65.

45. Liu, X., et al. *Low cost sensor network for indoor air quality monitoring in residential houses: Lab and indoor tests of two PM sensors*. 2016. 7th International Conference on Energy and Environment of Residential Buildings, November 20-24 2016, Brisbane, Australia.

46. Kumar, P., et al., *Real-time sensors for indoor air monitoring and challenges ahead in deploying them to urban buildings.* Science of the Total Environment, 2016. 560: p. 150-159.

47. Dye, T. *Using a Mobile Sensing System to Monitor Air Quality near Wildland Fires*. in *IAWF's 2nd International Smoke Symposium*. 2016. Long Beach California.

48. *Enabling Low-Cost Particulate Matter Measurement for Participatory Sensing Scenarios.*

49. Wang, Y., et al., *Laboratory Evaluation and Calibration of Three Low-Cost Particle Sensors for Particulate Matter Measurement.* Aerosol Science and Technology, 2015. 49(11): p. 1063-1077.

50. Volckens, J., et al., *Development and evaluation of an ultrasonic personal aerosol sampler*. Indoor Air, 2016.

51. *Christman Field Weather Station*. [cited 2016 8/15]; Available from: http://www.atmos.colostate.edu/wx/fcc/.

52. *U.S. climate data*. Available from: http://www.usclimatedata.com/climate/fort-collins/colorado/united-states/usco0140.

53. *Christman Field Weather Station*. Available from: http://www.atmos.colostate.edu/wx/fcc/.

54. *Engineering Design Guide and Environment*. [cited 2015 3/7/2015]; Available from: http://edge.rit.edu/edge/P11401/public/Concept%20Design%20Review%20Documents.

55. NF, C.R.S.J., *Pargin RX 2016 Monitoring Report*, F. Service, Editor. 2016.

56. *MesoWest*. Available from: http://mesowest.utah.edu/cgi-bin/droman/mesomap.cgi?state=CO&rawsflag=3.

57. *Environmental Dust Monitor #180 USER MANUAL*. Available from: http://www.lisa.u-pec.fr/~formenti/Tools/Manuals/GRIMM_model1.180_Manual_May04.pdf.

58. Mader, B.T. and J.F. Pankow, *Gas/solid partitioning of semivolatile organic compounds (SOCs) to air filters. 3. An analysis of gas adsorption artifacts in measurements of atmospheric SOCs and organic carbon (OC) when using Teflon membrane filters and quartz fiber filters.* Environmental science & technology, 2001. 35(17): p. 3422-3432.

59. Kirchstetter, T.W., C.E. Corrigan, and T. Novakov, *Laboratory and field investigation of the adsorption of gaseous organic compounds onto quartz filters.* Atmospheric Environment, 2001. 35(9): p. 1663-1671.

60. *Grimm Environmental Dust Monitor #180 User Manual*. Available from: http://www.lisa.u-pec.fr/~formenti/Tools/Manuals/GRIMM_model1.180_Manual_May04.pdf.

61. District, S.C.A.Q.M. [cited 2017 3-17]; Available from: http://www.aqmd.gov/aq-spec/evaluations/field.

62. Larsen, M., *Comparison of Particulare Monitoring Methods at Fort Air Partnership Monitoring Stations*. 2014, FAP.

63. Benton-Vitz, K. and J. Volckens, *Evaluation of the pDR-1200 real-time aerosol monitor*. Journal of occupational and environmental hygiene, 2008. 5(6): p. 353-359.

64. Radke, L.F., et al., *Airborne monitoring and smoke characterization of prescribed fires on forest lands in western Washington and Oregon: Final report*. 1990: US Department of Agriculture, Forest Service, Pacific Northwest Research Station.

65. Budde, M., et al. *Enabling low-cost particulate matter measurement for participatory sensing scenarios*. in *Proceedings of the 12th international conference on mobile and ubiquitous multimedia*. 2013. ACM.

66. Olivares, G. and S. Edwards, *The Outdoor Dust Information Node (ODIN)–development and performance assessment of a low cost ambient dust sensor*. Atmospheric Measurement Techniques Discussions, 2015. 8: p. 7511-7533.

67. Martins, J.V., et al., *Sphericity and morphology of smoke particles from biomass burning in Brazil.* Journal of Geophysical Research: Atmospheres, 1998. 103(D24): p. 32051-32057.

68. Soo, J.-C., et al., *Air sampling filtration media: Collection efficiency for respirable size-selective sampling.* Aerosol Science and Technology, 2016. 50(1): p. 76-87.

69. Russell, D.A.T., *Consultation on Monitoring Issues Related to the NAAQS for Particulate Matter* U.S.E.P. Agency, Editor.

APPENDICES

Power failure probabilities of the final OAS design consisting of 3 solar cells (0.014m^2 each) and 5 Li-ion batteries (10.78 Watt-hrs. each) for all months of the year is depicted in Figure 7-1. The simulation predicts an achievable continuous sampling length of 3 full days during December, January, February; 4-6 days for August, September, October, November, March, April and May; while June and July can sample for upwards of a full week continuously.

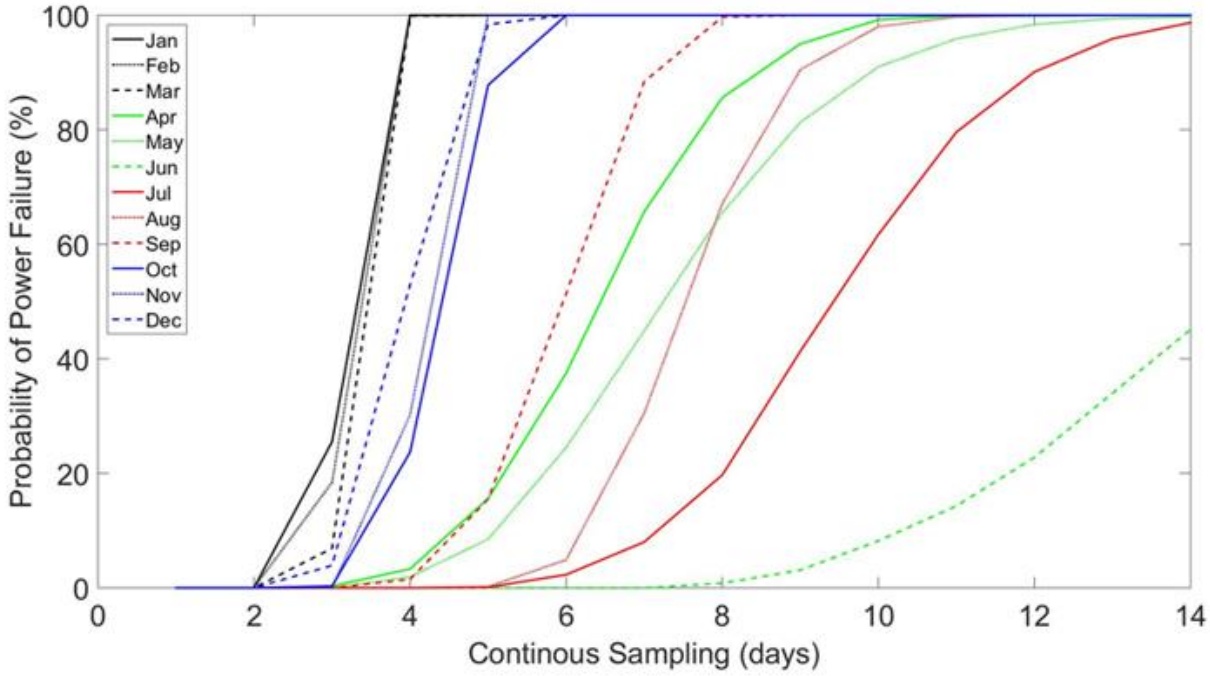

Figure 0-1. Monte Carlo simulation results showing OAS power failure probability for all months of the year. Axis define number of continuous sampling days and probability of power failure. Colors represent season.

The amount of runtime added back to the OAS via solar for each 24-hr sampling period during the prescribed fire sampling is shown in Figure 7-2. Solar irradiance shielding from fire smoke reduced the amount of energy reaching the OAS in some locations, thus reducing the amount of energy that could be stored and later used to extend runtime.

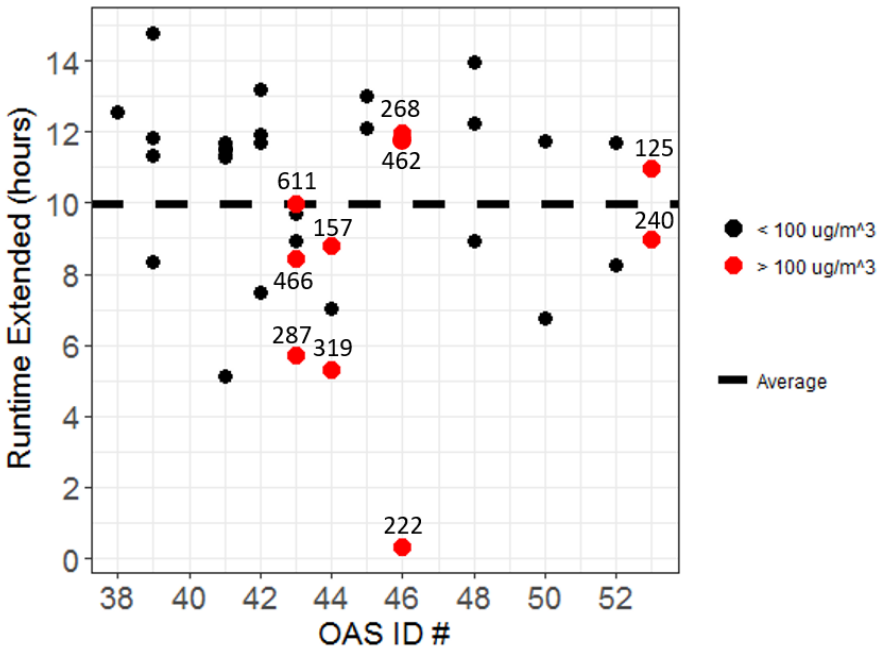

Figure 0-2. OAS runtime added via solar during prescribed fire sampling. Colors specify whether sampler was in high (red) or low (black) concentration for the duration of the sampling period. Axis represent hours of runtime added and sampler ID number.

Maps illustrating interpolated mass concentrations for the 24-hour prescribed fire sampling periods (September 15th and 17th) are represented in Figure 7-3. On Sept 15th Figure 7-3a, winds were light and variable. Concentrations were at or below NAAQS 24-hour average acceptable limit of 35µg/m^3 at the southern end of the sampling locations. At locations east of the fire, high concentrations were observed. On Sept 17th Figure 7-3b, wind was frequently from a northerly direction. Concentrations were extremely high at most locations and concentration gradients were strong.

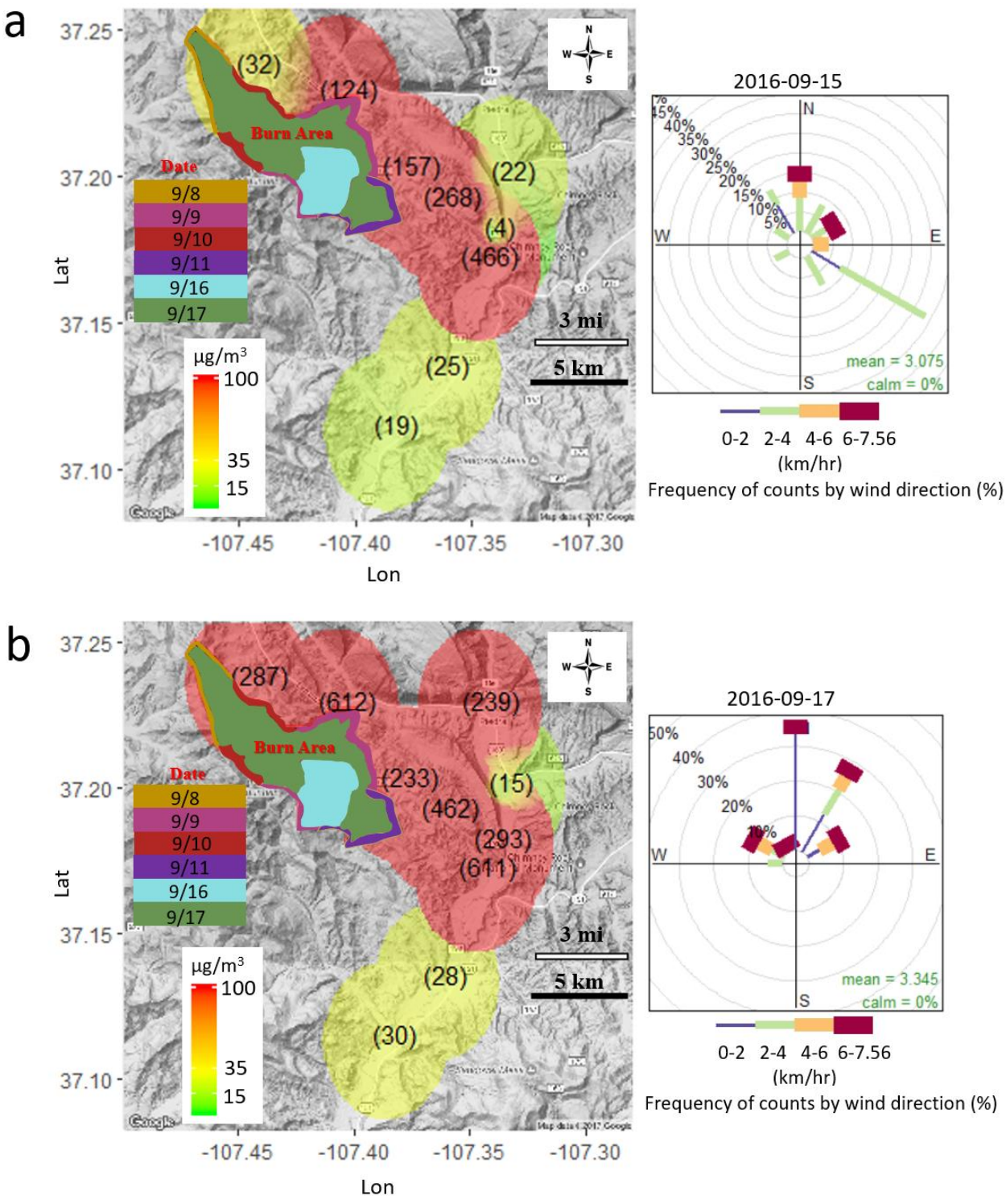

Figure 0-3. Maps illustrating spatial concentration gradients and the temporal evolution of fire emissions for Sept 15th, and 17th, 2016.

Tisch PTFE filter collection efficiency as a function of particle size is shown in Figure 7-4. Raw data is represented by black circles while average collection efficiency is depicted by a red line. The red

shaded area represents an estimated count distribution of fine particles produced by the prescribed fire while the blue shaded area represents the particle size distribution collected by the filter. The PTFE filters used were found to have a mass collection efficiency count collection efficiency of 68.2%.

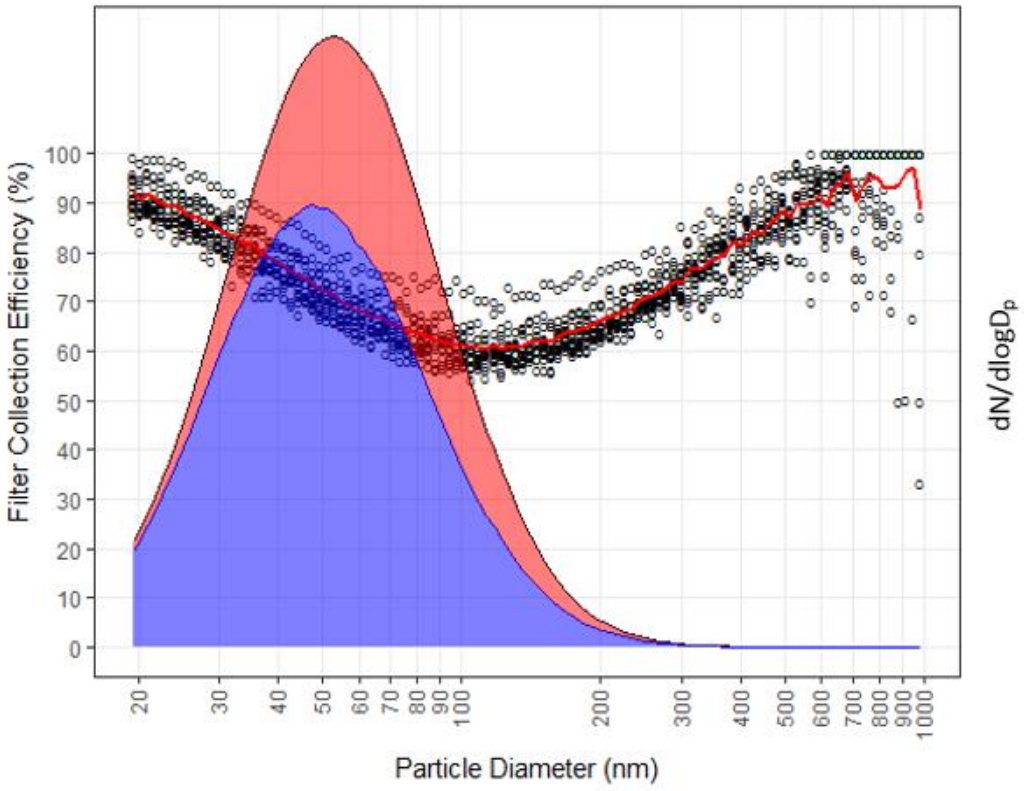

Figure 0-4. Collection efficiency of 37mm Tisch PTFE filters with respect to particle mobility diameter and count distribution of particles (red) and count distribution collected by the filters (blue). Primary vertical axis represents filter collection efficiency; secondary vertical axis represents change in particle count. Horizontal axis is particle size.

The particulate mass deposited on the sampling filters during the prescribed fire sampling campaign is shown in Figure 7-5. Mass accumulated ranged between 6 µg and 1722 µg. Of the 61 filters shown, 80.3% of the filters were above the limit of quantification (28.7 µg) and 85.2 % were above the limit of detection (17.3µg). These limits were based on 25 sampling filter blanks (5 filter blanks each sampling period).

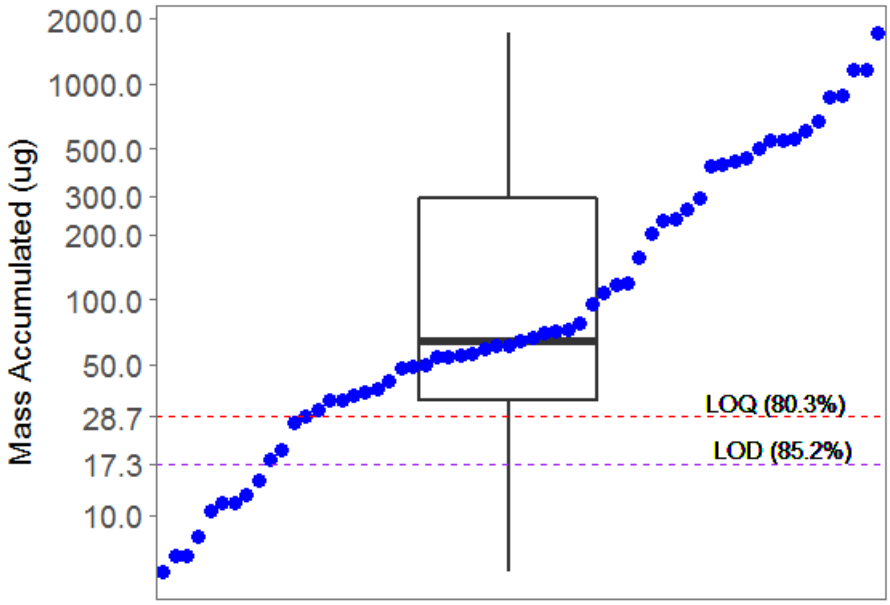

Figure 0-5. Mass deposited on sampling filters during the prescribed fire sampling campaign.

Forty-eight hour averages of urban sampling mass concentrations at each site are shown in Figure 7-6 for OAS and Grimm samplers. The concentration averages broken down by each sampling period and site is shown in Figure 7-7. The OAS is observed to over sample the Grimm at nearly all locations on 5 of the 7 periods. However, the OAS under sampled the Grimm at all 5 sites on 2017-02-02, and under sampled the Grimm at 3 sites on 2017-02-11. The date represents the day the 48-hour sample started. All sampling periods began at midnight and concluded at midnight 48-hours after sampling began.

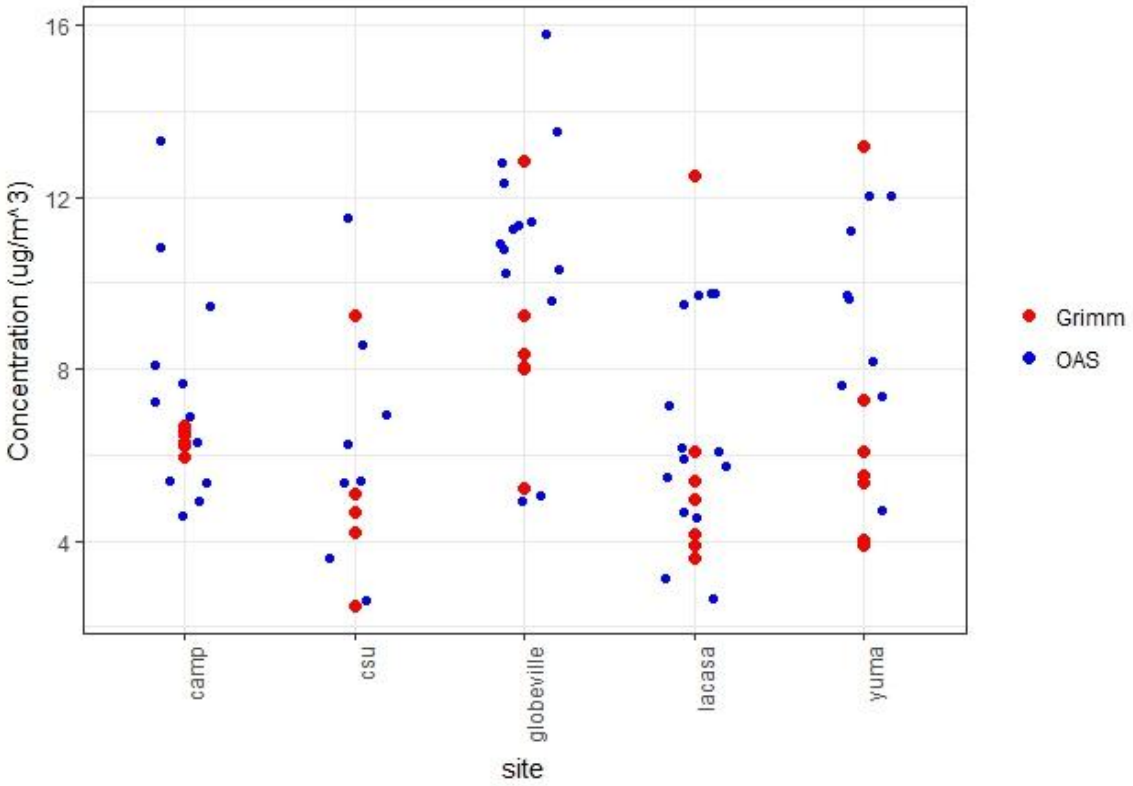

Figure 0-6. Forty-eight-hour average mass concentrations measured by Grimm and OAS for all 5 urban sampling sites.

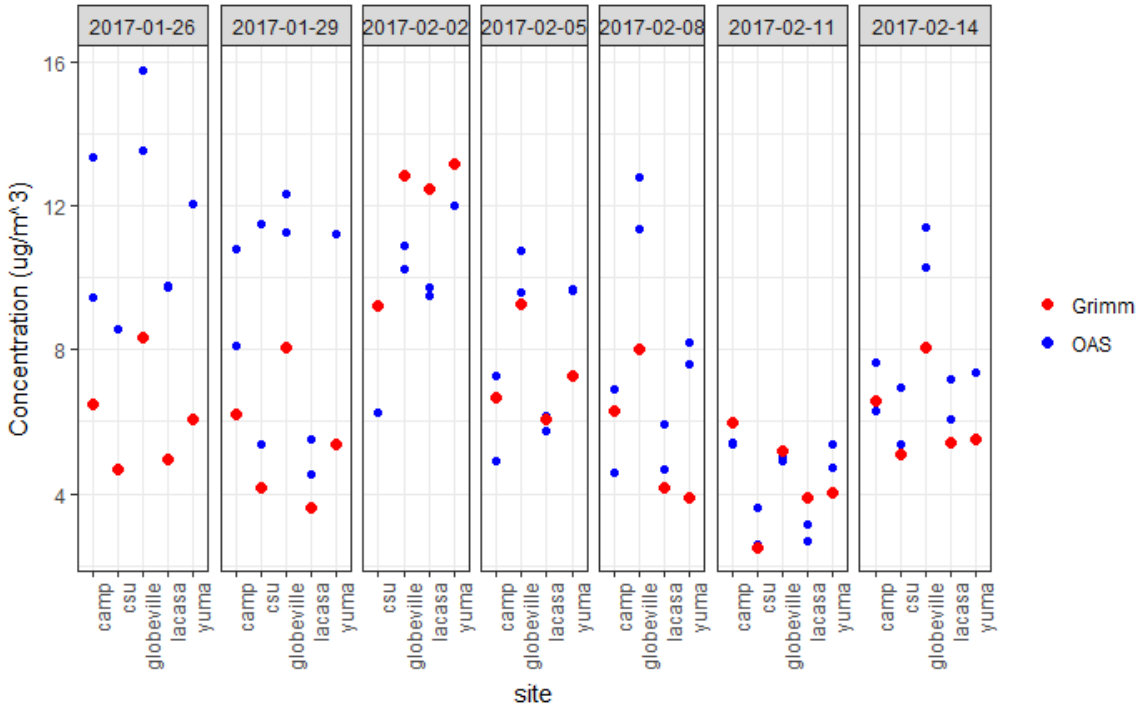

Figure 0-7. Forty-eight-hour average mass concentrations measured by the Grimm and OAS for each sampling period and site.

The mass deposited on the filters from urban sampling is represented in Figure 7-8. Mass accumulations range between 8µg and 90 µg. All filters were above the limit of detection (7.89 µg) and all but one filter were above the limit of quantification (13.15µg). The limits were based on 35 filed sampling blanks (5 sampling blanks each sampling period).

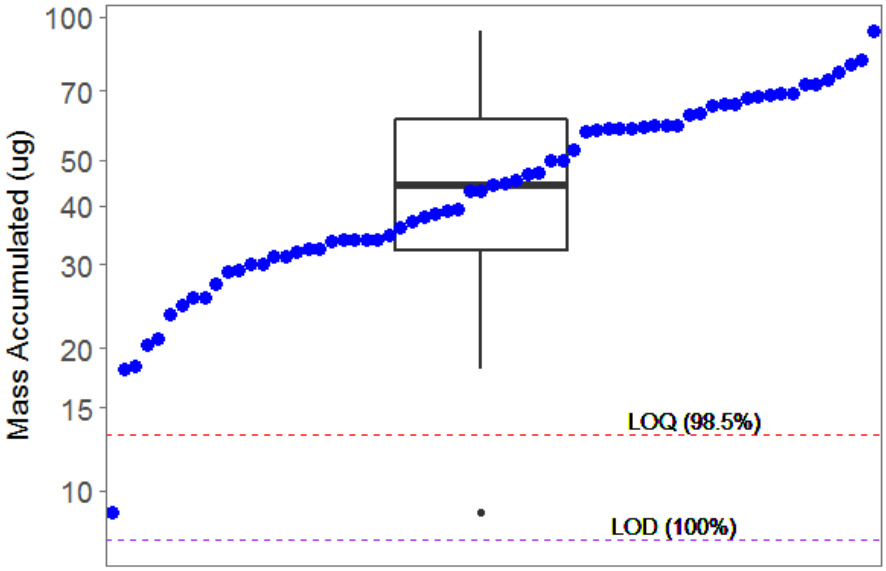

Figure 0-8. Mass deposited on sampling filters during the urban sampling campaign.

The number of acres burned, date burning occurred, and land area impacted is outlined in Figure 7-9. All burn dates refers to the date of ignition; continuation of burning and pollution emission may have occurred after date specified.

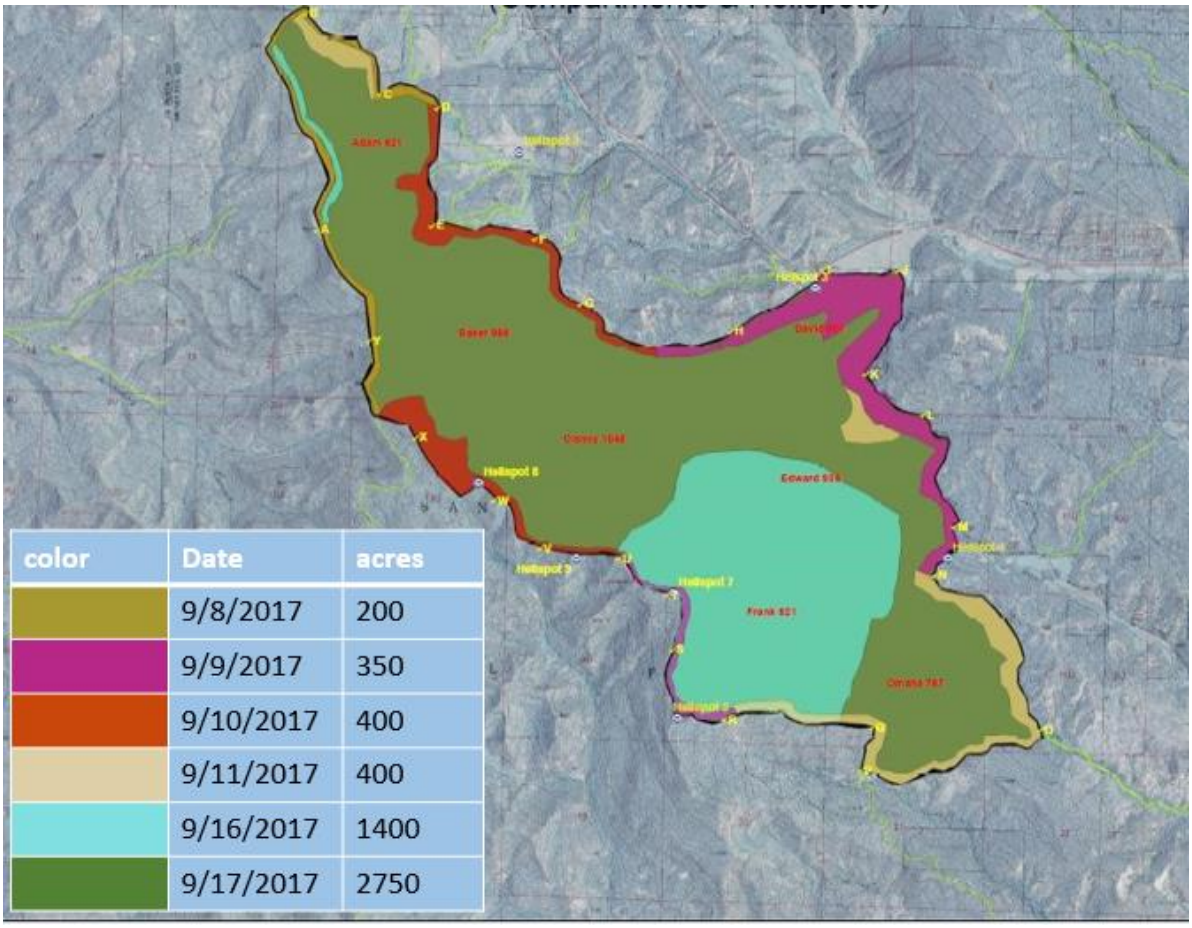

Figure 0-9. Map of fire depicting the burned area by date.

Fuel loading data collected by the USFS both pre and post burn using the Browns Fuels Transect Method is shown in Table 4. A Browns Fuels Transect estimates dead and down wood like material by tons per acre. Fuels recorded range from 1hr (0-.25”), 10hr (.25-1”) 100hr (1-3”), 1000hr (3+”) and litter and duff depths.

Table 4. Prescribed fire fuel loadings pre- and post-fire

Pre-burn Fuel Loading						Pre-burn Field Depth		
	1 hr	10hr	100hr	litter	duff	litter depth	duff depth	Total Fuel Load
Gambel Oak	0.21			3.08	1.98	0.75	0.1	5.27
Doug Fir	0.89	1.84	6.28	6.85	7.47	0.7	0.5	23.34
Ponderosa	0.23	0.96	2.55	1.17	9.53	0.38	0.6	14.45
Average	0.44	1.4	4.42	3.7	6.33	0.61	0.4	14.35
Post-burn Fuel Loading						Post-burn Field Depth		
	1 hr	10hr	100hr	litter	duff	litter depth	duff depth	Total Fuel Load
Gambel Oak	0.18			0.41		0.1		0.59
Doug Fir		4						
Ponderosa		0.96		0.7	1.99	0.23	0.13	3.65
Average	0.18	0.96		0.56	1.99	0.16	0.13	2.12